In Situ Water Vapor Measurements Using Coupled UV Fragment Fluorescence/Absorption Spectroscopy in Support of CRYSTAL-FACE

Summary of Research
NASA Goddard Grant NAG5-11548
Funding Period February 1, 2002–June 30, 2004

Submitted to
National Aeronautics and Space Administration
from
President and Fellows of Harvard College
c/o Office for Sponsored Research
Holyoke Center, Suite 727
1350 Massachusetts Avenue
Cambridge, Massachusetts 02138

James G. Anderson, Principal Investigator
Division of Engineering and Applied Sciences and
Department of Chemistry and Chemical Biology
Harvard University
12 Oxford Street
Cambridge, MA 02138

November 8, 2004

In Situ Water Vapor Measurements Using Coupled UV Fragment Fluorescence/Absorption Spectroscopy in Support of CRYSTAL-FACE

NASA Goddard Grant NAG5-11548. Summary of Research.
Funding period February 1, 2002–June 30, 2004

Understanding the coupling of dynamics, chemistry, and radiation within the context of the NASA Earth Science Enterprise (ESE) and the national Climate Change Science Program (CCSP) requires, as a first-order priority, high spatial resolution, high-accuracy observations of water in its various phases. Given the powerful diagnostic importance of the condensed phases of water for dynamics and the impact of phase changes in water on the radiation field, the accurate, *in situ* observation of water vapor is of central importance to CRYSTAL FACE (CF). This is clear both from the defined scientific objectives of the NRA and from developments in the coupled fields of stratosphere/troposphere exchange, cirrus cloud formation/removal and mechanisms for the distribution of water vapor in the middle/upper troposphere. Accordingly, we were funded under NASA Grant NAG5-11548 to perform the following tasks for the CF mission:

1. Prepare the water vapor instrument for integration into the WB57F and test flights scheduled for Spring 2002.
2. Calibrate and prepare the water vapor instrument for the Summer 2002 CF science flights based in Jacksonville, Florida.
3. Provide both science and engineering support for the above-mentioned efforts.
4. Analyze and interpret the CF data in collaboration with other mission scientists.
5. Attend the science workshop in Spring 2003.
6. Publish the data and analysis in peer-reviewed journals.

Field Performance

The water vapor instrument performed successfully on the NASA WB-57F research aircraft during the three test flights in May 2002 from Ellington Air Force Base, Houston, Texas; the ferry flight from Houston to Key West, Florida; and the 12 science flights in July 2002 from Key West Naval Air Station in Key West. In addition to the preflight laboratory calibrations performed at Harvard, calibration equipment was taken into the field and laboratory calibrations were carried out in both the Ellington Field and Key West Naval Station hangars. Instrument performance and accuracy is essential because quantitative measurements of water vapor in the upper troposphere and lower stratosphere are critical for understanding not only the radiative properties of this region but also the relationship between the microphysics of cirrus clouds, their lifetime, and the relative humidity in as well as outside the cloud. The measurements of relative humidity in cirrus clouds can be an issue because this instrument has an internal cell, with a residence time on the order of 15 milliseconds and is ram-heated by about 15°C, allowing for the possibility of particle evaporation.

Instrument Accuracy

In the context of the requirements for accurate water vapor measurements, it is important to assess the present state of atmospheric water vapor measurements. To address this we refer to Figure 1 from the SPARC Assessment of Upper Tropospheric and Stratospheric Water Vapor [SPARC 2000], the bottom third of which is shown here as Figure 1. This diagram summarizes the relationships between lower stratospheric water vapor measurements from different

instruments. We quote from the conclusion section of chapter 2 on data quality, with specific reference to this figure: "For both the troposphere and stratosphere there is no single technique or instrument platform that is recognized as a standard to which other techniques should be compared, and thus comparisons were made relative to one another."

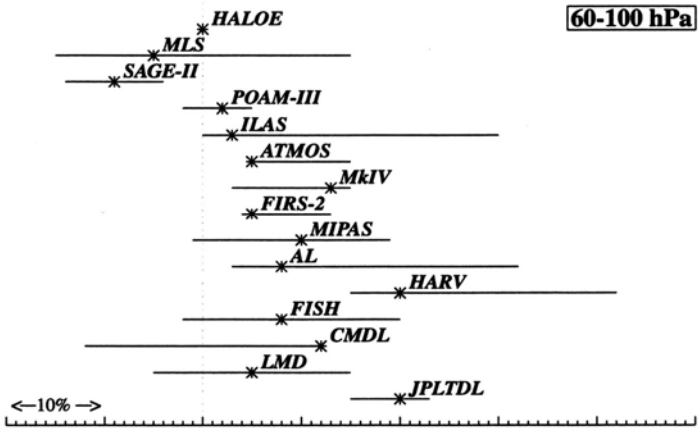

Figure 1. Reproduction of the bottom third of Figure 1 of the SPARC Assessment of Upper Tropospheric and Stratospheric Water Vapour [2000]. Data is plotted for each instrument as % difference from HALOE determined either from direct intercomparisons, represented by asterisks, or indirect comparison, represented by a horizontal line covering the range of disagreement. If the asterisk is centered on the line, it represents the average of the indirect intercomparisons.

So, what are the implications of this figure, how do we assess these implications, and why is it relevant to CF science? We first list and discuss the implications:

1. The figure suggests a potential uncertainty in water vapor measurements of at least 30% based on the spread in the data. However, this figure combines and accordingly places on an equal footing, *in situ*, remote, and space-based measurements with no regard for instrument pedigree or quoted accuracy. Satellite instruments are generally validated by intercomparison with *in situ* instruments. Their accuracy is, in fact, intrinsically limited by the accuracy of the validating instruments. The validation of remote instrumentation is inherently more difficult than that of *in situ* instrumentation. Nevertheless, even if we restrict ourselves to just comparing the *in situ* instruments, the spread in the measurement disagreement is still no better than 15%. Moreover, a recent intercomparison between the Harvard and JPLTDL [May *et al*., 1998] on the NASA WB57 during the Pre-AVE campaign with the balloon-borne CMDL frost-point instrument [Voemel H. *et al*., 2003] show the frost-point measuring lower than the aircraft instruments by about 1–1.5 ppmv, ~ 30–50% in the critically important tropopause region.
2. After about thirty years of instrument development, testing, validating, and intercomparing, no gold standard for water vapor measurements exists. This begs the question, "Are we making water vapor measurements accurate enough to satisfy the needs of the scientific and global communities?"
3. The Harvard and JPLTDL instruments appear as outliers, because they provide water vapor measurements that are systematically high. Independent analyses of systematic errors during CF, Pre-AVE, and the Midlatitude Cirrus experiment (MidCiX) indicate that this is not the case.
4. The assessment of instrument accuracy is primarily accomplished by the evaluation of instrument intercomparisons. This is a paradigm promulgated by a community that does not appear to be familiar with or accept the practice of adapting highly sensitive and well-calibrated laboratory instruments for robotic in-flight measurements. Well-developed laboratory techniques, when carefully and rigorously applied along with in-flight diagnostics

verifying the maintenance of established laboratory instrument sensitivity during the flight, must serve as the primary piece of evidence for instrument accuracy for *in situ* instruments.

The successful pursuit of the scientific issues that were the focus of the CF mission require measurements of water that are significantly more accurate than the SPARC figure suggests are currently viable. For example, the interpretation of observations of supersaturation in clear air and in clouds [Smith *et al*., 2004], and in contrails [Gao *et al*., 2004] in the context of understanding nucleation mechanisms and cloud microphysics require accurate water vapor measurements. A lack of confidence in these measurements would eliminate any hope of attacking the scientific issues that were the focus of the mission. Additionally, the accuracy of the determination of the ice water content of the cirrus clouds studied during CF is constrained by the accuracy of the water vapor measurements.

Water vapor instrument accuracy ultimately depends upon:

Point 1. The quality of the laboratory calibration.

Point 2. Maintaining and validating laboratory detection sensitivity in flight.

Point 3. Reliably transporting unperturbed ambient air to the detection region.

We use water vapor data taken during the CF mission by the water vapor, total water, and JPLTDL instruments to illustrate how the validation process relies on the consonance of careful laboratory calibrations (point 1) with in-flight diagnostics (point 2) and instrument intercomparisons (points 2 and 3). Additionally, we outline here our plan to improve both the accuracy and precision of our water vapor measurements with the goal of improving our benchmark quality water vapor measurements.

During the CF mission, a modified version of our laboratory calibration bench, shown in Figure 2, was brought into the field. In-field calibrations now augment the laboratory calibrations traditionally performed before and after the mission. The calibrations establish the sensitivity of the photofragment fluorescence detection axis to varying water vapor mixing ratios over a range of pressures and flow rates. The absolute calibration is tied to the vapor pressure of water at room temperature and corroborated with simultaneous (long-path) axial absorption at 121.6 nm at the detection axis as well. The convergence of these simultaneous determinations of the water vapor mixing ratio sets our confidence level for each calibration. (The calibration procedure is identical for both the water vapor and total water instruments).

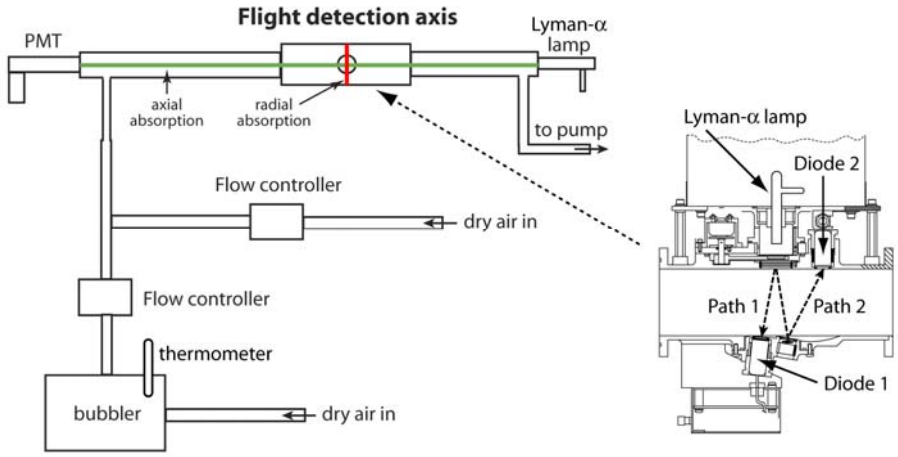

Figure 2. A schematic of the calibration system used in the laboratory and in the field. During calibration the detection axis, with the schematic representation of the components necessary for radial absorption shown on the right, is positioned within the flow tube where long-path axial absorption is carried out.

In-flight diagnostics for water vapor and total water must test points 2 and 3, listed above. For the water vapor instrument, with flow velocities of 40–80 m/sec, the first issue is confirmed by proving its insensitivity to a periodic factor of three change in the mass flow-rate through the instrument. The second issue is addressed by intercomparing the change in water vapor mixing ratio (delta water) as measured by fluorescence and absorption during constant altitude flight legs in the upper troposphere that fortuitously exhibit large mixing ratio excursions. Figure 2 shows an example of one such intercomparison. Similar in-flight intercomparisons were carried out during the STRAT and POLARIS campaigns with the functionally identical ER2 water vapor instrument [Hintsa *et al.*, 1999] and during CF with the total water instrument.

To address the issue of instrument accuracy we have searched for conditions during the flights where changes of water vapor mixing ratio during a level flight leg are significant enough to measure the change in water vapor mixing ratio by absorption. This allows for a comparison between water vapor measured by absorption and by photofragment fluorescence quantified by laboratory calibrations, validating point 2. Figure 3 shows an example where water vapor measured by the two techniques agree to within 5%. It is important to note that during the CF mission there were numerous examples of in-flight intercomparisons of total water measured by fluorescence and absorption that exhibited the same level of agreement shown in Figure 3, directly validating the in-flight calibration of the total water detection axis and through in-flight intercomparisons of the two measurements in clear air the calibration of the water vapor detection axis as well.

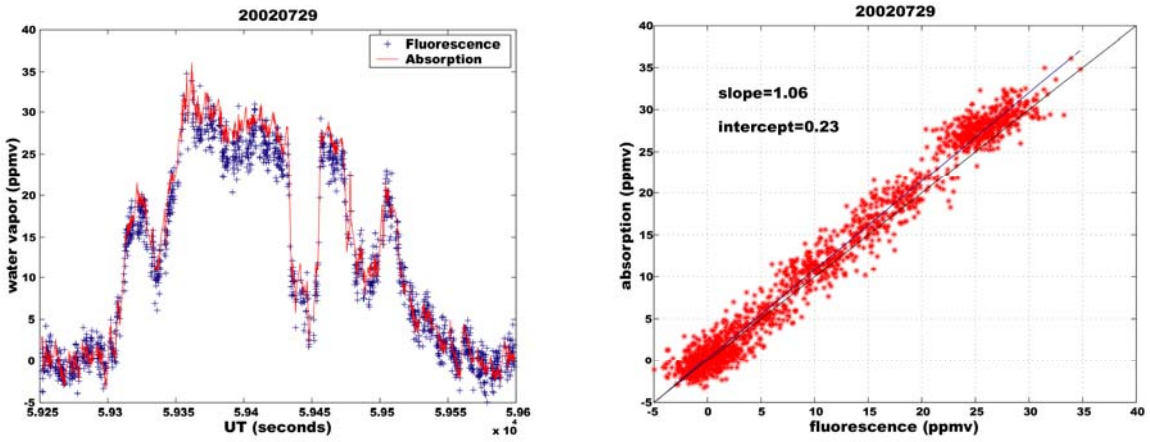

Figure 3. Intercomparison of water vapor measured by fluorescence and in-flight absorption on 20020729 during the CRYSTAL-FACE mission**.** The left-hand panel shows the detailed agreement between water vapor measured by absorption and fluorescence. The right-hand panel plots delta water measured by absorption versus fluorescence for the same data points plotted in the left-hand panel, as well as a linear least squares fit to the data (dotted line). Also plotted is the slope = 1 line for reference. The non-zero intercept is a result of the uncertainty in the data points before and after the absorption feature that are used to determine I_o.

Validation is exhibited for clear air measurements, by intercomparing with the JPLTDL hygrometer as well as our own water vapor instrument. We plot in Figure 4 an example of agreement exhibited during CF. This particular example illustrates agreement of the three water vapor measurements, and illustrates that in clear air neither the measurements of the *in situ* fast-flow water vapor instrument nor those of the slower flow (necessitated by the isokinetic inlet) total water instrument show evidence of perturbation or contamination by the instrument walls. These comparisons provide strong evidence for the accuracy of the detection axis.

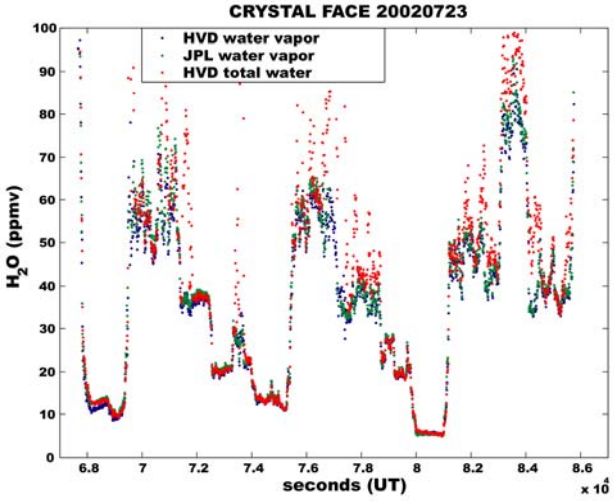

Figure 4. Comparison of water vapor instruments for the July 23, 2002, flight during the CF mission, showing agreement for the three instruments in clear air. The presence of clouds is evident during positive excursions by total water.

Particle Evaporation

To address particle evaporation in the water vapor inlet we take advantage of the existence of simultaneous measurements of water vapor by the JPL multipass laser diode hygrometer. This instrument uses an open cell design and is not subject to particle evaporation. While using preliminary data the two instruments do not agree, we adjust the JPL water vapor measurement to agree with ours in clear air and then compare measurements within clouds. In Figure 5 our water vapor instrument exhibits a measured increase in water vapor in clouds equivalent to about 5% of the ice water content of the cloud. This factor can be used to correct measured relative humidity within clouds using the Harvard water vapor instrument. We believe this amount of particle evaporation is caused by a light trap in the water vapor duct and this trap will be redesigned to alleviate the problem for the Tropical Clouds Systems and Processes (TCSP) mission in Summer 2005.

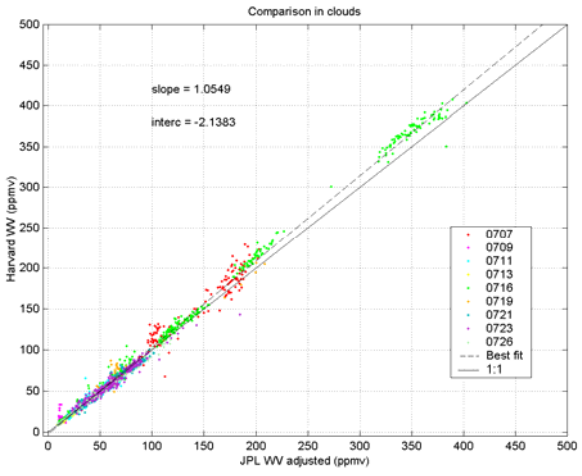

Figure 5. Plot of water vapor measured by the JPL diode laser hygrometer vs. the water vapor measured by the Harvard instrument. The JPL data has been adjusted such that it agrees with the Harvard data taken in clear air. The plot illustrates that the Harvard water vapor measures on average 5.5% high in clouds, apparently caused by particle evaporation in the instrument duct upstream of the detection axis.

Current Science and Data Analysis Initiatives

1. The CF mission was the first opportunity for simultaneous water vapor and ice water measurements in cirrus clouds in the upper troposphere. These measurements were a unique

opportunity to study the relationship between saturation or relative humidity within and around cirrus clouds and to investigate the dependence of supersaturation on particle size distribution, temperature, and tracer fields. As a first step in this study, analysis proceeded to quantify and validate the supersaturation using the water vapor and total water measurements. This was critical because supersaturations in cirrus clouds measured using preliminary data were significantly higher than expected, typically ranging from 120–150% and up to 180% at the coldest temperatures that are common at the tropical tropopause. These measurements provided significant constraints on the mechanisms that control the formation and evaporation of cirrus ice particles. When combined with relative humidity measurements taken during the Clouds and Water Vapor in the Climate System (CWVCS) and Pre-AVE missions in Costa Rica during Summer 2001 and Winter 2002, measurements of supersaturation have been made over a wide range of temperatures in the subtropics and tropical tropopause region. These measurements have significant implications on the *in situ* formation of thin cirrus and the dehydration mechanisms that might control stratospheric water vapor, as discussed by Jensen *et al*. [2004]. Smith *et al*. [2004] have examined the statistics of supersaturation as a function of temperature and show that homogeneous nucleation is the dominant mechanism in cirrus cloud formation with nucleation thresholds exhibiting a strong temperature dependence. Observation of in-cloud relative humidity appears to be sensitive to both temperature and cloud ice water content.

2. Understanding the mechanisms that control the water vapor budget of the upper troposphere is critical for input into global climate models. Because cirrus clouds represent a significant source of water in the upper troposphere, determining where and when those ice particles evaporate and tracing where that water ends up provides critical information for global climate models. These issues are under investigation using the simultaneous measurements of ice, water vapor, and other simultaneously measured tracers and are addressed under item 4, below.
3. Recently, interest in the middleworld, the extratropical region bound from above by the 380 K isentropic surface and from below by the local tropopause, has peaked because of recent trends in midlatitude ozone loss as well as the concern that aircraft effluent might somehow become part of the general circulation. There is also significant interest regarding the potential growth of water vapor in this region as the climate warms both because of its radiative impact as well as the potential for heterogeneous ozone loss on cloud surfaces formed in regions of high water vapor. The CF mission represents the first opportunity to develop a significant database of tracer measurements in the middleworld in the summer and at this longitude. This is particularly interesting because the summer monsoon that sets up off the coast of the Pacific provides a mechanism for the equatorward flow of air in the upper troposphere and lower stratosphere. This flow provides a potential mechanism for the flow of air from northern latitudes into the tropical tropopause layer from where that air can become part of the general circulation and rise into the lower stratosphere. Pittman *et al*. [2004] have examined the results of 3-D back trajectories and tracer-tracer correlations in the lowermost stratosphere during CF to explore the impact of the western monsoon on the composition of the observed air. The authors identified three transport regimes from back trajectory calculations that show consistency with the changing tracer-tracer correlations and the monsoon circulation.
4. As an extension of the Pittman *et al*. [2004] analysis, we used the tracer data obtained during CF and a simple box model to determine what fraction of this air is stratospheric, recently

having descended from the lower stratosphere; what fraction is stratospheric, having descended in northern latitudes and then traveled equatorward as part of the monsoon circulation; what fraction originated in the upper tropical troposphere; and what fraction is due to local or northern latitude convection [Weinstock *et al*., 2004]. The model shows that not only is there a significant fraction of old stratospheric air entrained in the monsoonal circulation, but that for the entire month of July convection is a significant contributor to the lowermost stratosphere in the air measured over south Florida. This information is critically relevant to point two, above, illustrating a method of measuring the impact of cirrus clouds on the water vapor budget of the upper troposphere and lower stratosphere. Water vapor is measurably increased even up to 380 K and with the equatorward flow there is significant potential for this moist air to enter the Brewer Dobson circulation. The analysis also illustrates that, in summer, midlatitude ozone depletion is subject to the influence of many factors that could be influenced by climate change. On the one hand, convection significantly moistens the tropopause region and lowers the temperature at which clouds can either form or increases the lifetime of those that have formed by increasing the relative humidity in the region. The potential increase in NO_x and other convectively transported pollutants means that increased homogeneous ozone loss must be considered as well. While significant increases in NO were not measured above the local troposphere during CF, the model indicates significant NO_y from a convective source between 360–380 K. This NO_y originates as lightning induced NO and accordingly could be a significant source of ozone loss in the lowermost stratosphere. Modeling this loss would be complicated by the added HO_x from enhanced water as well as the potential presence of organics such as formaldehyde, acetone, and methyl peroxide. On the other hand, analysis shows how the potential for changes in the relative importance of different transport pathways for air into the lowermost stratosphere could easily cause the observed variability in ozone in this region. In either case, the coupling of monsoonal flow and convective activity can significantly complicate modeling ozone in the midlatitude lowermost stratosphere in summer.

Summary

From an instrumental standpoint, one of the most important achievements of our CF measurements was establishing the paradigm that the accuracy of *in situ* water vapor measurements in the UT/LS is directly linked to the accuracy of laboratory calibrations and confirmation that the laboratory calibration is valid in flight. This, of course, has always been an accepted requirement for the Harvard photofragment fluorescence hygrometer but was thought to be less of an issue—if an issue at all—for multipass IR laser absorption hygrometers. Based on our laboratory calibrations and in-flight validations using direct absorption of Lyman-α radiation, and agreement in clear air between the water vapor and total water instruments, we have established 5% accuracy of the instrument. In clouds, we have determined that there can be an approximately 5% evaporation of particles in the duct because of ram heating. We will redesign the instrument duct to alleviate this problem before the TCSP mission.

The accurate measurement of water vapor and other tracers during the CF mission has provided the means to carefully study a number of issues relating midlatitude ozone depletion, cirrus cloud formation, evolution and lifetime, the stratospheric water vapor budget, and the impact of the summer monsoon on the lowermost stratosphere. In the appendix we include preprints of two papers soon to be submitted on these topics.

References

R. S. Gao, *et al*., Measurements of relative humidity in a persistent contrail, *J. Geophys. Res*., submitted, 2004.

Hintsa, E. J., E. M. Weinstock, J. G. Anderson, and R. D. May, On the accuracy of *in situ* water vapor measurements in the troposphere and lower stratosphere with the Harvard Lyman-α hygrometer, *J. Geophys. Res*. **104**, 8183–9, 1999.

May, R. D., Open-path, near-infrared tunable diode laser spectrometer for atmospheric measurements of H_2O, *J. Geophys. Res.* **103**, 19,161–72, 1998.

Jensen, E., *et al*., Measurements of ice saturation exceeding 100% at the cold tropical tropopause: Implications for ice nucleation, cirrus formation, and dehydration, *J. Geophys. Res*., submitted, 2004.

Smith J. B. *et al*., Observations and implications of supersaturation in clear air and in the presence of cirrus in the tropical and subtropical stratosphere, in preparation, 2004.

SPARC Assessment of Upper Tropospheric and Stratospheric Water Vapour, WCCRP N° 113, WMO/TD-N° 1043, December 2000.

Vomel, H. *et al.,* Balloon-borne observations of water vapor and ozone in the tropical upper troposphere and lower stratosphere, *J. Geophys. Res.* **108**, doi: 10.1029/2002JD002984, 2003.

Appendices

Pittman, J. V. *et al*., Identifying transport pathways into the subtropical lowermost stratosphere during the summertime, *J. Geophys. Res.*, in preparation, 2004.

Weinstock, E. M. *et al*., Quantifying the impact of the North American monsoon and deep midlatitude convection on the subtropical lowermost stratosphere using *in situ* measurements on the NASA WB57 during the CRYSTAL FACE campaign, *J. Geophys. Res.*, in preparation, 2004.

Identifying transport pathways into the subtropical lowermost stratosphere during the summertime

Jasna V. Pittman,[1] Elliot M. Weinstock,[1] David S. Sayres,[1] Jessica B. Smith,[1] James G. Anderson,[1] Owen R. Cooper,[2] Steven C. Wofsy,[1] Irene Xueref,[1] Cristoph Gerbig,[1] Bruce C. Daube,[1] Erik C. Richard,[2] Karen H. Rosenlof,[2] Brian A. Ridley,[3] Andrew Weinheimer,[3] Max Loewenstein,[4] Hans-Jürg Jost,[4] Jimena P. Lopez,[4] Michael J. Mahoney,[5] and Thomas L. Thompson[2]

Abstract.

We use in situ measurements of water vapor (H_2O), ozone (O_3), nitric oxide (NO), total reactive nitrogen (NO_y), carbon monoxide (CO), carbon dioxide (CO_2), and methane (CH_4) obtained during the Cirrus Regional Study of Tropical Anvils and Cirrus Layers - Florida Area Cirrus Experiment (CRYSTAL-FACE) campaign in July 2002 aboard NASA's WB-57 aircraft along with 3-D backward trajectory calculations to identify transport pathways into the subtropical lowermost stratosphere. This region of the stratosphere is bounded from below by the local tropopause coincident with the 360 K isentrope over Florida during this campaign and from above by the tropical tropopause or the 380 K isentrope. The high spatial and temporal resolution that in situ measurements provide allow us to track changes in the chemical composition of this region throughout the month. Correlation plots of tracers with respect to H_2O in clear air show evidence of three major transport pathways bringing air into the subtropical lowermost stratosphere, namely equatorward transport of high-latitude stratospheric air, poleward transport of upper tropical tropospheric air, and convectively driven transport from both local and non-local events. These transport pathways identified by tracer correlations are consistent with 3-D backward trajectories in both the geographical origin of the air sampled over Florida and the timing of the dominant large-scale transport pathway. The equatorward transport has been associated with monsoon circulation. In this work we present evidence of the effect of this circulation on the chemical composition of the lowermost stratosphere over North America using O_3-H_2O correlations from the CRYSTAL-FACE and the Stratospheric Tracers of Atmospheric Transport (STRAT) campaigns during the summer. These results provide new insights into the spatial and temporal resolution of the dynamics of the subtropical lowermost stratosphere during the summertime. Understanding the dynamics of this region of the atmosphere is crucial for predicting the radiative and chemical impacts of long-term changes in O_3 and H_2O in the stratosphere.

1. Introduction

Understanding the coupling between chemistry and dynamics in the atmosphere during all seasons is crucial for accurately predicting the future of the global climate system and the impact of any potential changes on human health and the environment. Effective policies rely on accurate predictions. Such predictions while necessary are very challenging, because they require not only understanding the underlying physics and chemistry, but also understanding coupling and feedback mechanisms that can account for the effects of both natural variability and anthropogenic activity.

One of the irrefutable human-induced changes in the climate system has been the erosion of the ozone layer in the stratosphere over the last two decades. The evolution and formation of the stratospheric ozone hole over the poles during late winter and early spring is a prime example of the result of coupling of chemistry (local reactions) and dynamics (transport of gases and aerosols to the poles and isolation of air masses in the polar vortex). Numerous studies of this phenomenon have ultimately led to a better understanding of the winter stratosphere. The summer stratosphere, on the other hand, has not been studied extensively because it has been regarded as quiescent due to the weakening of the large-scale circulation driven by thermal forcing and wave activity [*Plumb*, 2002]. Lacking this knowledge hinders our ability to fully understand and predict the impact of changes in the chemistry and dynamics of the atmosphere as a result of year-round greenhouse gas and aerosol emissions resulting from anthropogenic activity.

Besides polar regions, decreases in stratospheric ozone have also been observed at midlatitudes. The latest report on the Assessment of Ozone Depletion shows that between 1983 and 2001 the annual total column of ozone in both Northern and Southern Hemisphere midlatitudes was 2 to

[1]Department of Earth and Planetary Sciences, Harvard University, Cambridge, Massachusetts, USA.

[2]Aeoronomy Laboratory, National Oceanic and Atmospheric Administration, Boulder, Colorado, USA.

[3]Atmospheric Chemistry Division, National Center for Atmospheric Research, Boulder, Colorado, USA.

[4]NASA Ames Research Center, Moffett Field, California, USA.

[5]Jet Propulsion Laboratory, Pasadena, California, USA.

0148-0227/04/$9.00

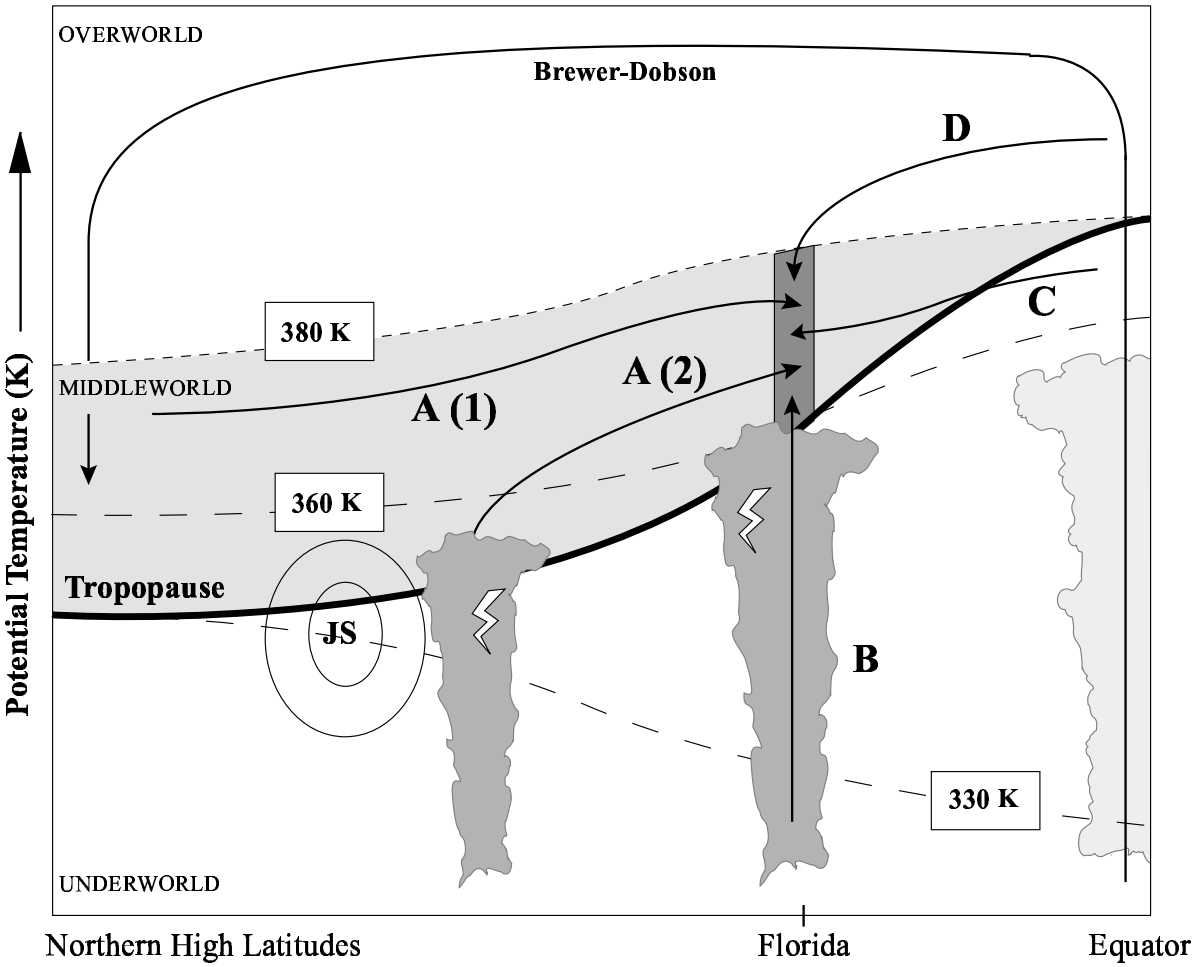

Figure 1. Possible transport pathways of air into the lowermost stratosphere over Florida (gray box): A(1) equatorward transport of stratospheric air, A(2) equatorward transport of convective air injected into the stratosphere at higher latitudes, (B) local convection, (C) poleward transport of upper tropical tropospheric air, and (D) diabatic descent from the tropical stratosphere. JS represents the approximate location of the polar jet stream during July 2002. The subtropical jet stream is not observed during this time of the year. The light gray shading represents the lowermost stratosphere.

8% lower than the mean calculated during the period 1964-1980 with the last four years still showing reductions in the order of 3% in the global mean total column ozone [WMO, 2002]. On a seasonal time-scale, the largest losses occur during winter and spring with deviations from the 1964-1980 mean as large as 12% in 1992-1993. Ozonesonde data from middle and high latitudes in the Northern Hemisphere quantify the ozone loss as a 7% decrease per decade between 1970 and 1996 with the maximum loss occurring in the lowermost stratosphere during the spring [*Logan et al.*, 1999]. The abundance of ozone in this region can be controlled by in situ chemistry and by transport of ozone-poor air (processed springtime polar air and tropospheric air) [WMO, 2002]. Therefore, it is necessary to characterize the composition of the lowermost stratosphere at these latitudes and explore the dynamical processes that influence this region in order to understand how the abundance of stratospheric ozone might vary in response to climate change.

The pioneering work of *Brewer* [1949] and *Dobson* [1956] proposed the existence of a mean meridional circulation where air enters the stratosphere primarily through the tropical tropopause, and it returns to the troposphere at high latitudes. This large-scale circulation, known as the Brewer-Dobson circulation, links different regions of the lower atmosphere. According to *Hoskins* [1991], these regions correspond to the overworld, the middleworld, and the underworld. In the overworld and underworld, air is considered to be entirely in the stratosphere and troposphere, respectively. In the middleworld, air is considered to be in the troposphere at low latitudes and in the stratosphere at high latitudes. The boundaries for each of the three regions are set by isentropes or surfaces of constant potential temperature. In this study, we look at measurements obtained on the stratospheric side of the middleworld, which is known as the lowermost stratosphere. This region is bounded from below by the local tropopause, and from above by the 380 K isentrope, which nominally corresponds to the tropical tropopause.

Exchange of air masses between the troposphere and the stratosphere occurs all year round with certain pathways having a seasonal dependence. In this work, we use an Eulerian approach to study the dynamics of the summer lowermost stratosphere using in situ measurements of H_2O, O_3, NO, NO_y, CO, CO_2, and CH_4 obtained during the Cirrus Regional Study of Tropical Anvils and Cirrus Layers - Florida Area Cirrus Experiment (CRYSTAL-FACE) in July 2002.

The possible transport pathways that brought air to the lowermost stratosphere in the subtropics during CRYSTAL-FACE are shown in Figure 1. Pathway A corresponds to

isentropic transport of tropical stratospheric air that descended diabatically at high latitudes and traveled equatorward quasi-isentropically. Equatorward transport can carry either pure stratospheric air (pathway A(1)), or a mixture with tropospheric air recently injected into the stratosphere via middle- or high-latitude convection (pathway A(2)). Pathway B corresponds to direct penetration of local convection. Pathway C corresponds to isentropic transport of upper tropical tropospheric (UTT) air across the subtropical tropopause. In this study we refer to the subtropical tropopause as the tropopause break or the tropopause found between the tropics and Florida. Lastly, pathway D corresponds to isentropic transport from the tropical stratosphere followed by diabatic descent into the subtropical lowermost stratosphere.

Evidence of these transport pathways has been reported in previous studies. For instance, a recent analysis of ozone profiles during CRYSTAL-FACE shows layers of high ozone in the subtropical lowermost stratosphere, which have been associated with large-scale equatorward transport of high-latitude air into the subtropics (pathway A(1)) [*Richard et al.*, 2003]. A climatological study using 21 years of rawinsonde data shows that this type of transport is expected in areas located to the east of monsoon regions, in this case the North American Monsoon, as a result of the circulation around the upper level quasi-stationary anticyclone that develops during the summer [*Dunkerton*, 1995]. A study using a semi-Lagrangian transport model also shows the existence of this transport pathway adjacent to monsoon regions and qualifies it as very active during the summer [*Chen*, 1995]. In terms of convection, summertime observations show tropospheric air reaching into the lowermost stratosphere (pathway A(2) and B) [*Poulida et al.*, 1996; *Vaughan and Timmis*, 1998; *Jost et al.*, 2004]. Late spring aircraft measurements [*Dessler et al.*, 1995; *Hintsa et al.*, 1998] as well as modeling studies [*Chen, 1995*; *Dethof et al.*, 2000; *Stohl et al.*, 2003] have provided evidence for isentropic transport of air from the UTT (pathway C). Finally, a combination of satellite and aircraft measurements of ozone have shown that diabatic descent into the lowermost stratosphere (pathway D) is strongest during late winter and early spring and weakest during the summer and the fall [*Prados et al.*, 2003]. Calculations of the residual mean meridional circulation have also shown that diabatic descent into the lowermost stratosphere takes place at latitudes north of the jet stream with a maximum occurrence during winter and minimum occurrence during summer [*Rosenlof*, 1995].

This study has two main objectives. The first objective is to use two independent approaches to identify the pathways in Figure 1 that broght air into the lowermost stratosphere over Florida during CRYSTAL-FACE. The first approach is to use tracer correlations of O_3, NO, NO_y, CO, CO_2, and CH_4 with respect to H_2O (vapor only). H_2O is very sensitive to temperature and it can be used to distinguish stratospheric air (very dry) from tropospheric air (wet) in the lowermost stratosphere. The difference in mixing ratios between these two regions is particularly useful when studying a region of strong and frequent convection that can bring tropospheric air into the stratosphere. The second approach is to calculate 3-D backward trajectories. Trajectory calculations are based on assimilated meteorological fields that can be useful in identifying the dominant transport pathway associated with the large-scale circulation. Therefore, a combination of in situ measurements, minimum temperatures and trajectory calculations allow us to obtain a more comprehensive picture of the dynamics in this region by combining the high spatial and temporal resolution of tracer measurements with the wide spatial coverage of trajectories.

The second objective is to investigate the impact of the monsoon circulation on the chemical composition of the lowermost stratosphere given the evidence of equatorward transport of high-latitude stratospheric air to Florida [*Richard et al.*, 2003] and the geographical proximity of this location to the monsoon region. For this purpose, we use in situ measurements of H_2O and O_3 obtained during two campaigns. These campaigns are CRYSTAL-FACE based out of Florida in July 2002, and Stratospheric Tracers of Atmospheric Transport (STRAT) based out of California in July and out of Hawaii in August 1996. Even though the measurements from these two campaigns are six years apart, their geographical location is key to our analysis.

2. Methods

2.1. Measurements

We use in situ measurements obtained aboard two different NASA's high-altitude research aircraft during the campaigns shown in Figure 2. We focus this study on the analysis of data obtained on the WB-57 aircraft during CRYSTAL-FACE. This campaign was based out of Key West, Florida during July 2002 and accomplished 12 flights over 27 days. We restrict our analysis to data collected in the lowermost stratosphere over the southern Florida region between 24°N and 27°N and 77°W and 85°W. We exclude the last flight (July 29) in this analysis due to the existence of two tropopauses: one at approximately 12 km, which was over 2 km below the average location of the local tropopause and another at approximately 16 km, which was coincident with the location of the 380 K isentrope during this campaign. This variability in location made it difficult to specify the boundaries for the lowermost stratosphere during this flight.

In order to achieve the first goal in this study, we use the following tracer measurements: H_2O measured by the Harvard hygrometers which are based on Lyman-α photofragment fluorescence [*Weinstock et al.*, 1994], O_3 measured by dual-beam UV absorption [*Proffitt and McLaughlin*, 1983], CH_4 measured by near IR absorption using a tunable diode laser [*Richard et al.*, 2002], NO and NO_y measured by chemiluminescence [*Ridley et al.*, 1994], CO measured by IR absorption using a tunable diode laser [*Loewenstein et al.*, 2002], and CO_2 measured by nondispersive IR absorption [*Daube et al.*, 2002]. All tracer data are averaged over 10 seconds, which gives a horizontal resolution of 1.8 km along the flight track.

We use the Microwave Temperature Profiler (MTP) instrument [*Denning et al.*, 1989] to locate the local

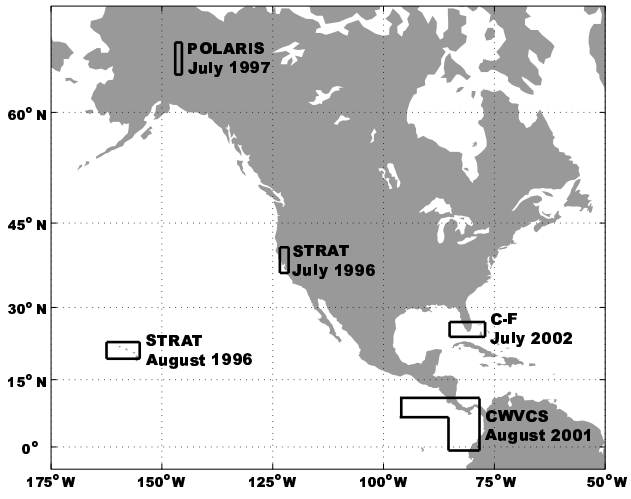

Figure 2. Geographical location of all aircraft campaigns used in this study.

tropopause. This instrument uses the World Meteorological Organization (WMO) definition of the tropopause (i.e., minimum altitude where -dT/dz is less than 2 K/km over a region of 2 km in depth). Location of the local tropopause using in situ measurements of pressure and temperature made by the PT instrument [*Thompson and Rosenlof*, 2003] and application of the WMO definition yielded results that agreed well with those reported by MTP.

For this analysis, we select clear-air data in the lowermost stratosphere. We use a combination of calculated saturation water vapor mixing ratio from PT and in situ ice content derived from the difference of water measured by the Harvard Total Water and the Harvard Water Vapor instruments to identify and remove occasional cloud data found in this region. The lower boundary for the lowermost stratosphere or the local tropopause was found around the 360 K isentrope over Florida during the month of July (between 14.4 km and 15.6 km, or 147 hPa and 121 hPa) and the upper boundary or the tropical tropopause corresponding to the 380 K isentrope was found between 15.2 km and 16.2 km (127 hPa and 110 hPa) over Florida.

In order to achieve the second goal in this study, we use comparable measurements of H_2O, O_3, and tropopause location obtained aboard the ER-2 aircraft during the STRAT campaign. These measurements were obtained out of California in July 1996 and out of Hawaii in August 1996.

Besides these two campaigns, we also use in situ measurements from two other campaigns in our analysis. These campaigns are: Photochemistry of Ozone Loss in the Arctic Region in Summer (POLARIS) based out of Fairbanks, Alaska in July 1997 and Clouds and Water Vapor in the Climate System (CWVCS) based out of Costa Rica in August 2001.

2.2. Trajectory Model

Backward trajectories for selected flights during CRYSTAL-FACE are calculated using the Forward And Backward trajectory (FABtraj) model. This is a diabatic model that uses NCEP Final Analysis (FNL) wind fields and a linear interpolation scheme in space and time. The meteorological dataset used is available every 6 hours and it has a horizontal grid resolution of 1°x1° and a vertical resolution of 21 levels between 1000 and 100 hPa. The vertical levels are prescribed in sigma (or terrain-following) coordinates.

The FABtraj model has been used in studies of synoptic scale midlatitude cyclones and has been compared to trajectory models such as FLEXTRA [*Cooper et al.*, 2004]. The comparison shows a 7% difference in median horizontal distance traveled after 5 days. Because of the strong convective activity during CRYSTAL-FACE, we choose to use a diabatic model instead of an adiabatic model in order to properly link the troposphere and the stratosphere at middle and high latitudes where isentropic surfaces are contained in one of the two regions only. Additionally, air parcels that are advected back in time for more than a few days experience some degree of heating or cooling during this time of year, especially when traveling over or through regions of strong and frequent convective activity. This condition affects the entropy of the air parcel and makes their trajectories non-adiabatic for periods longer than a few days.

3. Results and Discussion

3.1. Tracers

Each of the source regions for the four major transport pathways depicted in Figure 1 has a distinct chemical signature. In order to obtain reference values in each source region, we use both aircraft data and surface measurements. The aircraft data were obtained during the campaigns shown in Figure 2. The surface measurements were obtained from NOAA's Climate Monitoring and Diagnostics Laboratory Carbon Cycle and Greenhouse Gases (CMDL CCGG) group at various locations in the tropics and midlatitudes.

The tracers, location, and reference for the representative values for each source region are summarized in Table 1. The representative values of the chemical composition of each source region are presented in Table 2. Any reference to H_2O from this point forward corresponds to the vapor phase only.

The data representative of the high latitude lowermost stratosphere come from the POLARIS campaign only. This air is not pure stratospheric, but a mixture of stratospheric air from the overworld and tropospheric air from the underworld instead. Since the equatorward transport pathway is quasi-isentropic, we would expect air of this composition to be the source instead of a pure stratospheric air from the overworld. The tropospheric component in these air masses can be variable, so we use the POLARIS measurements with caution. The CO_2 values reported in Table 2 for this campaign have been corrected to account for the secular increase in the atmosphere between the POLARIS and the CRYSTAL-FACE missions.

Very limited measurements of the chemical composition of convective air in the upper troposphere and lower stratosphere (UTLS) have been reported [*Poulida et al.*, 1996; *Ridley et al.*, 2004]. A recent study of a convective event that took place on July 16, 2002 during CRYSTAL-FACE shows that convective air that reached the UT over Florida had a fraction of boundary layer air and a fraction of free tropospheric air entrained into the convective updraft [*Xueref et al.*, 2004]. Since these two fractions are variable from one cloud to another, we use the values shown in Table 2 as examples of the composition of air that has been observed to reach the UTLS.

In terms of the UTT, the reported values in Table 2 come from direct aircraft observations except for H_2O and CO_2, which were estimated. The H_2O values represent minimum and maximum saturation mixing ratios at the local tropopause between the Equator and 15°N and 0° and 180°W during July 2002. We derived average values of tropopause pressure and temperature from the National Center for Environmental Prediction/National Center for Atmospheric Research (NCEP/NCAR) Reanalysis dataset and calculated the saturation mixing ratio using the Clausius-Clapeyron equation. Uncertainty in NCEP/NCAR tropical temperatures were accounted for by subtracting 2 K [*Shah and Rind*, 1998]. Observations of H_2O in the UTT during STRAT and CWVCS showed ranges between 8 and 15 parts per million by volume (ppmv) at 360 K, and 4 and 9 ppmv at 380 K, which are not that different from the values we obtained using NCEP/NCAR data. The values for CO_2 were estimated using surface measurements at Mauna Loa and Samoa during 2002, applying the global CO_2 clock [*Boering et al.*, 1996], and propagating the signal into the UTT with a 1 to 2-month lag with respect to surface values at the time of the campaign.

The values reported in Table 2 for the tropical lower stratosphere source come mostly from observations except for CO_2. We estimate the range of CO_2 using the same approach we took for the UTT source with the difference that the signal in this source region has a 4 to 6-month lag with the surface as *Boering et al.* [1996] reported.

The chemical lifetimes of all of these tracers are used to separate observed changes in mixing ratios due to chemistry from changes due to dynamics in the lowermost stratosphere over Florida during CRYSTAL-FACE. All tracers except NO have chemical lifetimes ranging from several months to several years. NO, on the contrary, has a chemical lifetime of one week in the UTLS during the summer [*Ridley et al.*, 1996]. This shorter lifetime can help us identify air in the

Table 1. Location and reference for origin of values that represent each source region shown in Figure 1. LmS stands for lowermost stratosphere, and LS for lower stratosphere. The difference between these two regions in the stratosphere is that the LmS is found below the 380 K isentrope while the LS starts above 380 K.

Source	Tracer(s)	Isentropes (K) or Lat–Lon(°)	Reference
High latitude LmS	All	360–380 K	POLARIS
Convection	O_3, CO	345–360 K	Poulida *et al.*, 1996
	O_3, NO_y, NO	350–370 K	Ridley *et al.*, 2004
	CO_2, CH_4	13°–42°N, 59°–155°W	Surface Measurements
UTT	H_2O	0°–15°	NCEP/NCAR Reanalysis
	H_2O, O_3	360–380 K	STRAT[a], CWVCS
	NO_y, NO, CO	360–380 K	STRAT[a], CRYSTAL-FACE[b]
	CO_2	360–380 K	Surface Measurements, Boering *et al.*, 1996
	CH_4	360–380 K	STRAT[a]
Tropical LS	H_2O, O_3	380–420K	STRAT[a], CWVCS
	NO_y, NO	380–420 K	STRAT[a], CRYSTAL-FACE[b]
	CO, CH_4	380–420 K	STRAT[a]
	CO_2	380–420 K	Surface Measurements, Boering *et al.*, 1996

[a] Reference values were measured during the flights based out of Hawaii only.

[b] Reference values were measured during the 20020709 and 20020726 flights where latitudes were <15°N.

lowermost stratosphere that was influenced by convection within a week prior to its detection over Florida. This observation along with other tropospheric tracers such as CO would suggest that convective influence is not only associated with local events, but also with events that originate elsewhere and get transported long distances via some pathway (A or C from Figure 1) that leads to Florida over the course of a week.

In order to explore the chemistry and dynamics of the lowermost stratosphere over Florida, we look at tracer correlations with respect to H_2O. The advantage of relating all tracers to H_2O is that this tracer shows a strong gradient across the tropopause due to its sensitivity to temperature changes. The temperature dependence of this tracer is reflected in observed mixing ratios of only a few ppmv in the stratosphere and observed mixing ratios up to four orders of magnitude larger near the surface. This difference is the result of a freeze-drying mechanism that air masses experience when they cross regions of cold temperature (e.g., tropopause, convective updrafts, UTT) as they travel from the troposphere to the stratosphere. In addition to its temperature sensitivity, H_2O has few sources and sinks and a lifetime of 100 years in the lower stratosphere [*Brasseur and Solomon*, 1986], which makes it a good tracer for transport.

The use of chemical tracers can help constrain the latitudinal origin of air masses. In this study we use O_3, NO_y, NO, CO, CO_2, and CH_4. O_3 can distinguish tropospheric from stratospheric air based on low and high values, respectively. NO_y represents total reactive nitrogen ($NO + NO_2 + HNO_3 + PAN + ...$) which can be used to distinguish tropospheric air from stratospheric air based on low values in the troposphere, especially in non-convective or old-convective air masses where NO is low. It can also distinguish the latitude of the stratospheric component based on lower values in the tropics and higher values at higher latitudes where N_2O gets photolyzed and oxidized to NO_y over time. NO is produced both in aircraft exhaust and by lightning during strong convection. Since the measurements we analyze were obtained 4 to 6 km above the altitude where commercial airliners fly, then observed increases in NO above background levels suggest the presence of convective air in the stratosphere. During the flight of July 13, the aircraft sampled its own contrail where NO values were near 2000 parts per trillion by volume (pptv). Most of these measurements took place below the tropopause, and the few that were located above the local tropopause were excluded from this analysis.

CO is another tracer that can be used to identify tropospheric air in the stratosphere where lower mixing ratios are found. This tracer has a lifetime of four months in the UTLS during the summer [*Crutzen et al.*, 1994] and in the stratosphere its primary loss is due to oxidation by OH. In the troposphere, CO can reach very high values as a result of incomplete combustion during biomass and fossil fuel burning. Observations of high values of CO in the stratosphere would suggest that a fast pathway (e.g., convection) must have lofted these air masses from the surface. CO_2 can separate old air (lower values) from young air (higher values) in the lowermost stratosphere, although the variability in its values can be attributed to other reasons as well. This tracer does not have major sources or sinks in the stratosphere, so its variations in the stratosphere are due to seasonal changes associated with photosynthesis and respiration in the biosphere and annual increases due to burning of fossil fuels. Finally, CH_4 can also be used to distinguish old air (lower values) from young air (higher values). This tracer does not have a seasonal cycle signature nor a significant annual increase in the stratosphere at the present, so lower stratospheric values are mainly driven by chemical loss due to oxidation by OH. By combining all the reviewed information provided by each tracer, we can constrain the origin of the air masses sampled over Florida during CRYSTAL-FACE.

3.2. CRYSTAL-FACE Tracer Correlations

Tracer-tracer correlation plots are useful in identifying the character of the sampled air masses based on how the

Table 2. Representative values of trace gases from each of the four source regions shown in Figure 1. All ranges except the ones in the Convective source are listed as observed values at the top followed by values at the bottom of each region specified in Table 1.

Source	H_2O(ppmv)	O_3(ppbv)	NO_y(pptv)	NO(pptv)	CO(ppbv)	CO_2(ppmv)	CH_4(ppbv)
High latitude LmS	4–10	600–300	2800–2000	170–250	21–35	368.7–370.5	1500–1600
Convection	10s–100s	60–120	200–4000	100–2000	80–140	369–374.5	1740–1785
UTT	4.8–12	160–40	1300–200	400–120	45–70	372.8–373.8[a]	1650–1750
Tropical LS	4.5–9	400–150	1500–500	250–500	25–45	371.4–373.4[a]	1640–1710

[a] This range represents extreme values expected within the source region and might not necessarily occur at the upper and/or lower boundaries of the LmS.

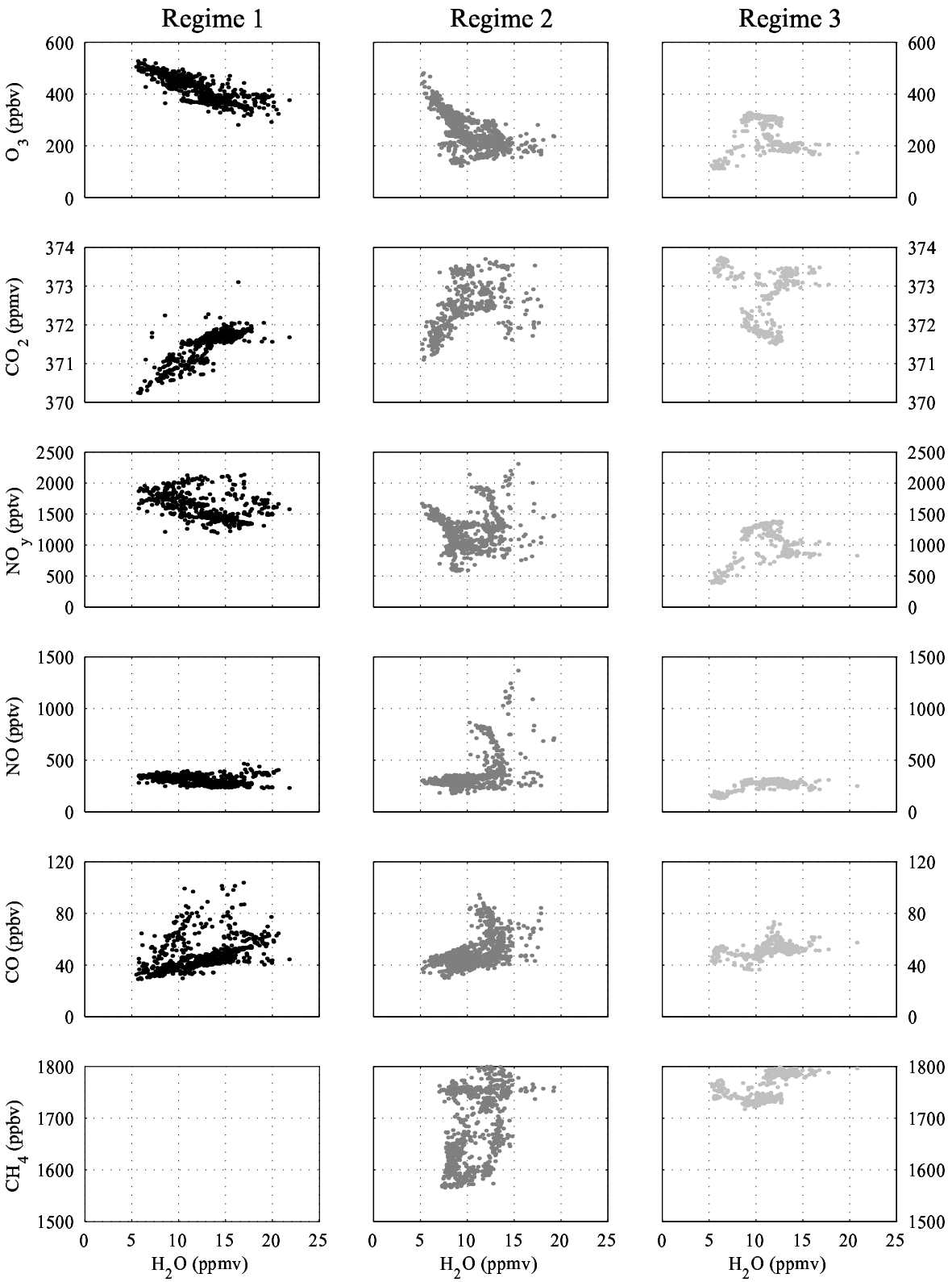

Figure 3. Correlations with respect to H_2O of O_3, CO_2, NO_y, NO, CO and CH_4 for each regime during CRYSTAL-FACE in July 2002. The black points correspond to regime 1, the dark gray points to regime 2, and the light gray points to regime 3. See text for regime definitions.

measurements compare to representative values from the troposphere and from the stratosphere during the same time of the year. Air masses with chemical compositions that are not representative of one region alone result from some level of mixing of air masses from different regions.

For the tracers we use in this study, we expect to see positive correlations with respect to H_2O for NO, CO, and CH_4, and negative correlations with respect to H_2O for O_3, and NO_y. The correlation plot between H_2O and CO_2 should have a positive correlation during the summer; however, it can be variable due to the dependence on the tropospheric source for CO_2 (e.g., maritime versus continental, tropics versus high latitudes). In the positive correlation plots, both H_2O and the given tracer have high values in the troposphere and low values in the stratosphere, so mixing between these two regions will show air masses with varying compositions that fall along a line with a positive slope. In the negative correlation plots, H_2O has a high value and the given tracer has a low value in the troposphere and H_2O has a low value and the tracer a high value in the stratosphere, so air masses with different fractions from both regions fall along a line with a negative slope.

When plotting all tracer-H_2O correlations, we observe three distinct regimes as shown in Figure 3. These regimes in tracer space correspond to the following flight dates: regime 1 from the 3^{rd} until the 9^{th} of the month, regime 2 from the 11^{th} until the 21^{st} of the month, and regime 3 from the 23^{rd} until the 29^{th} of the month.

3.2.1. Regime 1

In order to identify source region(s) where air masses sampled over Florida originated from, we consider all tracer-H_2O correlations shown in Figure 3. At first glance, the O_3-H_2O and the CO_2-H_2O correlations during this regime show fairly compact correlations along what appears to be one main mixing line. This implies that these air masses are mixtures of tropospheric and stratospheric air. The remaining correlation plots do not show clearly that this was the case, therefore we should explore each individual correlation plot in order to extract more detailed information.

During this regime, H_2O ranged from 5.5 to 22 ppmv. Air masses with the lowest H_2O levels are consistent with expected stratospheric values and can come quasi-isentropically from either high latitudes or the tropics (A(1) or D from Fig. 1). These low H_2O levels are also found in the UTT (C from Fig. 1) according to Table 2. Air masses with more than 10 ppmv of H_2O in the lowermost stratosphere are most likely to be of convective origin (A(2) or B from Fig. 1), but they could also come from the UTT where summertime values are variable. For these air masses with H_2O greater than 10 ppmv, the relative humidity varied from 30% to 120% and they were found between the local tropopause and 375 K. Of these air masses, 98% had relative humidities below 100%, which suggests that even though the lowermost stratosphere is wet, it is mostly undersaturated. The 2% air masses that were supersaturated were found right above the local tropopause, which implies that processes other than freeze-drying by the tropopause controlled the humidity of these air masses. This tracer alone tells us that air in this region had both tropopsheric and stratospheric character, but since various mechanisms and conditions can affect the humidity level of an air mass H_2O alone cannot distinguish the tropospheric source regions.

When looking at the O_3-H_2O correlation, we notice that the driest air masses contained 530 parts per billion by volume (ppbv) while the wettest air masses contained 300 ppbv. Air masses with the highest levels of O_3 and lowest H_2O must originate from the stratosphere at either high latitudes or the tropics (A(1) or D from Fig. 1). Air masses with this signature were found between 372 and 380 K. Because of the high levels of O_3, the stratospheric origin of these air masses is most likely to be from high latitudes instead of the tropics (see Table 2). A negative gradient in O_3 along with a positive gradient in H_2O as altitude decreased towards the tropopause suggests the presence of a tropospheric source that is diluting the O_3 mixing ratios and is increasing H_2O. This tropospheric air can come from a convective source or from the UTT (A(2), B, or C from Fig. 1), but there is no clear evidence based on these two tracers that can identify the origin of this component.

Turning to CO_2-H_2O, we find a positive correlation with CO_2 ranging from 370.25 ppmv to 373.1 ppmv. The lowest mixing ratios were found at the top of the region (379.6 K). According to reference values in Table 2, this low CO_2 over Florida can originate either from high latitudes in the stratosphere or from forested regions in the boundary layer where photosynthesis is taking place during this time of the year. If the air originated from forested regions, then convection must have lofted it into the stratosphere. This pathway, however, would carry more than 5.6 ppmv of H_2O into the stratosphere. Therefore, CO_2 levels at the top of the region point at stratospheric high latitudes as the origin of air over Florida. The positive correlation between these two tracers suggests that tropospheric air was present in the lowermost stratosphere as well. Since the tropospheric sources (A(2), B and C from Fig. 1) have very comparable values of CO_2, it is not possible to identify the latitudinal origin of the air mass based on this correlation alone.

The NO_y levels during this regime ranged from 1200 to 2200 pptv. The high values were mostly found in the driest air masses, which is consistent with stratospheric air coming from high latitudes where high levels of NO_y are found (A(1) from Fig. 1). During the flight of July 7, air masses with 10 to 20 ppmv of H_2O contained 1600 to 2200 pptv of NO_y, which is 25% more NO_y than during the other flights in this regime, and suggests convective influence. Although not as compact as the O_3-H_2O correlation, NO_y and H_2O were also anti-correlated suggesting the presence of both stratospheric and tropospheric air in the region.

NO looks fairly flat during this regime as seen in Figure 3; however, there are a couple of features in this correlation worth mentioning. First, NO stayed below 400 pptv for most of the regime even at the high H_2O mixing ratios. This observation is in agreement with a stratospheric source at the low H_2O values and a tropospheric source that was either not influenced by lightning or influenced by lightning more than a week earlier. Second, NO increased up to 500 pptv at the highest H_2O, which happened on July 7. The highest NO values were not coincident with the highest NO_y values during this flight. On the contrary, the highest NO mixing ratios had the lowest NO_y mixing ratios. Furthermore, the highest NO mixing ratios were found above the tropopause (360 K) while the highest NO_y mixing ratios were found between 366 K and 376 K. Air masses with high H_2O, high NO_y, and low NO point at a tropospheric source that if influenced by lightning, the influence happened a week prior to our detection. This timing would allow conversion of lightning-generated NO to NO_y.

During this regime, CO ranged from 29 to 104 ppbv. At the top of the region, we find again the driest air masses with the lowest CO mixing ratios (lower than 45 ppbv). These low-CO and low-H_2O air masses are characteristic of stratospheric air. On the flight of July 7, however, CO of up to 73 ppbv along with 6 ppmv of H_2O was found at 375 K. This was the upper edge of a plume that contained up to 104 ppbv of CO and 17 ppmv of H_2O between 368 and 376 K. The source for this high CO was identified as boundary layer air brought up by midlatitude convection associated with forest fires in Canada and the midwestern section of the U.S. [*Jost et al.*, 2004] (A(2) from Fig. 1). These results support the hypothesis suggested by the NO_y, NO, and H_2O measurements. With decreasing altitude towards the tropopause, air masses contained both higher H_2O and CO, which suggests presence of tropospheric air. Due to the variability of CO in the troposphere, the latitudinal origin of the source region cannot be clearly identified using this tracer.

Based on all tracer-H_2O correlations (CH_4 was not available during this regime), we conclude that the dominant pathways that transported air to the lowermost stratosphere over Florida during regime 1 were equatorward transport of high-latitude stratospheric air (low H_2O, high O_3, high NO_y, low NO, low CO, and very low CO_2) and tropospheric air (high H_2O, higher NO than background levels, and high CO). Excluding the event observed on July 7, air masses with more than 10 ppmv of H_2O were observed from the tropopause up to the 375 K isentrope, which correspond to the lower 1.2 km of a lowermost stratosphere that was 1.6 km in depth during regime 1. The plume of high CO observed on July 7 provided evidence for extratropical convection that penetrated into the stratosphere and then traveled equatorward towards Florida (A(2) from Fig. 1). Other than this event, the tracers-H_2O correlations shown in Figure 3 did not provide conclusive evidence for the origin of the tropospheric air observed in the lowermost stratosphere over Florida (A(2), B, or C from Fig. 1).

3.2.2. Regime 2

As the month progressed, Figure 3 shows how some correlation plots maintained evidence of mixing lines (i.e., O_3-H_2O, CO_2-H_2O and NO_y-H_2O) but with more scatter than during regime 1. Recall that these four tracers have long lifetimes, thus the scatter in the plots suggests that fast transport processes were influencing this region.

H_2O ranged from 5 to 20 ppmv similar to the range observed during regime 1. It is important to note that during this regime the local tropopause was at higher altitudes and colder temperatures. This condition decreased the saturation mixing ratio at the tropopause. The air masses that had more than 10 ppmv of H_2O showed relative humidities from 50% to 150% and were also found up to 375 K. Considerably less air masses were undersaturated during this regime (63%) compared to regime 1. The air masses that were supersaturated (37%) were found up to the 372 K isentrope with the highest supersaturation levels concentrated up to 4 K above the local tropopause during the flight of July 13. These results show that the local tropopause is not controlling the humidity of the region aloft. As previously discussed, this tracer alone can only show that the air masses in the lowermost stratosphere over Florida had both stratospheric and tropospheric sources. It cannot clearly distinguish the latitudinal origin of each source.

During this regime, the O_3-H_2O correlation showed a steeper slope with O_3 mixing ratios lower (450 ppbv) than during regime 1 in the driest air masses. The full range for this tracer was 120-450 ppbv. There are two potential case scenarios that can be responsible for the observed mixing ratios in this correlation. One case scenario is that the same sources during regime 1 were present during regime 2, but with a higher tropospheric fraction during regime 2. The higher tropospheric fraction acted to reduce the high O_3 mixing ratios found in high-latitude stratospheric air. The other case scenario is that instead of having high-latitude stratospheric air, the air came from the tropical stratosphere where O_3 levels are lower. Based on measurements shown in Table 2, values of 450 ppbv would have to come from potential temperatures higher than 420 K before descending diabatically to the lowermost stratosphere over Florida. The latter case scenario would imply a shift in the large-scale dynamics from equatorward to poleward transport of air into the lowermost stratosphere over Florida between regime 1 and regime 2.

In terms of CO_2, higher values (about 2 ppmv) were observed during this regime. This tracer ranged from 371 to 374 ppmv. The driest air masses with less than 5.5 ppmv of H_2O contained less than 371.6 ppmv of CO_2. The range for CO_2 mixing ratios in these air masses falls between the values of high-latitude stratospheric air and tropical stratospheric air according to Table 2. Therefore, these two tracers alone cannot clearly distinguish the stratospheric source region. Increasing values of CO_2 along with increasing values of H_2O as we descend towards the tropopause suggest the presence of tropospheric air in the lowermost stratosphere. Tropospheric CO_2 is very variable and its origin is hard to determine especially when multiple locations might contribute to the bulk observations shown in Figure 3. Thus, these two tracers alone cannot provide any additional information other than the presence of both stratospheric and tropospheric air in this region.

During regime 2, NO_y ranged from 540 to 2200 pptv. The maximum value was the same during regimes 1 and 2, but the minimum value during regime 2 was close to half of the minimum value during regime 1.

The highest mixing ratios of NO_y were found in the wettest air masses, which suggests that the air was influenced by convection. The driest air masses contained over 1500 pptv of NO_y, which suggests the presence of high-latitude stratospheric air over Florida. The minimum values observed suggests that either tropical air (tropospheric or stratospheric) or convective air strongly influenced this region during this regime as shown in Table 2. These air masses contained a wide range of H_2O (8 to 20 ppmv). The wettest air masses are consistent with air of convective origin that was not influenced by lightning (high H_2O and low NO_y).

Thus far, tracer-H_2O correlations suggest larger fractions of tropospheric air present in the lowermost stratosphere compared to regime 1. When we turn to the NO-H_2O correlation in Figure 3, we immediately see presence of recent convective air making it into the lowermost stratosphere. For H_2O less than 10 ppmv, NO does not show any difference in the character of the air compared to what we sampled during regime 1, which suggests that the source(s) of air did not change. For H_2O more than 10 ppmv, NO increased almost by a factor of three compared to regime 1 and it reached up to 372 K with the highest values (more than 1000 pptv) between 363 K and 369 K on the flight of July 21. These high NO values are clear evidence of the presence of convective air in the lowermost stratosphere, and based on the NO mixing ratios it appears to be local and recent convection. GOES-8 images show that at the time the aircraft was flying above the remnants of a single convective cell, which peaked in height and strength four hours prior to the aircraft encounter. Convection, however, could have reached the stratosphere either locally or non-locally (A(2), B, or C from Fig. 1).

Another good tracer for convection is CO. During regime 2, it ranged from 30 to 84 ppbv. Even though CO reached a minimum of 30 ppbv, most of the dry air masses (less than 8 ppmv of H_2O) contained 40 to 50 ppbv of CO, which is 10 to 20 ppbv higher than during regime 1. Compared to regime 1 and excluding the known plume with high CO that we observed on July 7, air masses with comparable H_2O throughout the region had 5 to 35 ppbv more CO during regime 2. These observations suggest a strong signature of tropospheric air in the lowermost stratosphere during this regime.

Lastly, we consider the CH_4-H_2O correlation. CH_4 ranged from 1565 to 1814 ppbv. Surface measurements obtained from the CMDL CCGG group over North America and the eastern and central Pacific during 2002 ranged from 1735 to 1980 ppbv of CH_4. Levels as low as 1565 ppbv observed in the lowermost stratosphere over Florida show significant loss of CH_4 compared to surface measurements. Once in the stratosphere, CH_4 is oxidized by OH but this process takes months to years. Therefore, air masses that contained such low levels of CH_4 in the lowermost stratosphere over Florida must have come from higher latitudes in the stratosphere (A(1) from Fig. 1) where we can find

the oldest air masses of all four source regions that we are considering . The wettest air masses during this regime had CH_4 levels comparable to surface measurements over North America, which suggests that convection (A(2) or B from Fig. 1) could have been the pathway into the stratosphere. However, the variability of CH_4 in each of the tropospheric source regions shown in Table 2 makes it difficult to clearly identify the origin of the tropospheric air.

Summarizing all the information obtained from tracers-H_2O correlation plots, we conclude that the dominant pathways that transported air to the lowermost stratosphere over Florida during regime 2 were still equatorward transport of high-latitude stratospheric air (low H_2O, high O_3, high NO_y, low NO, low CO, low CO_2, and low CH_4) and convection (high H_2O, high NO, and high CO). Air masses with H_2O greater than 10 ppmv were observed up to the 375 K isentrope, which corresponds to the lower 900 m of a lowermost stratosphere which was 1 km in depth during this regime. The stratospheric component was weaker than during regime 1 due to what appears to be a larger fraction of convective air in the region (higher NO, higher CO, and higher CH_4).

3.2.3. Regime 3

The tracer-H_2O correlations during this regime are different from the previous two regimes. Except NO, all tracers have longer chemical lifetimes than the time required for the transport pathways that we consider to reach our region of study. Therefore, the different correlations during this regime suggest a change in the dynamics during this regime.

Air masses had H_2O ranging from 5 to 22 ppmv similar to both regimes 1 and 2. The local tropopause relaxed back to similar altitudes to those observed during regime 1. The lowermost stratosphere was entirely undersatured during this regime with relative humidities as high as 75% near the tropopause and decreasing to as low as 15% below the 380 K surface. As previously discussed, this tracer alone can only show that the air masses in the lowermost stratosphere over Florida had both stratospheric and tropospheric sources despite the low relative humidities.

The O_3 mixing ratios during this regime ranged from 105 to 330 ppbv, which was 100 to 200 ppbv lower on the high end of the range compared to regimes 1 and 2. The maximum O_3 observed suggests that either high-latitude stratospheric air or tropical lower stratospheric air was present over Florida (A or D from Fig. 1). A combination of a small fraction of high-O_3 air (stratospheric) with a large fraction of low-O_3 air (tropospheric) could result in the observed values during this regime. The lowest O_3 mixing ratios suggest the presence of tropospheric air in the region. Approximately 30% of the air masses sampled during this regime had 105-150 ppbv of O_3, 5 to 7 ppmv of H_2O, and were found between 375 and 380 K. H_2O is too low to come from extratropical or local convection (A(2) or B from Fig. 1) and carry more than 100 ppbv of O_3, which leaves the UTT as the most probable tropospheric source (C from Fig. 1). In addition to the UTT, the tropical lower stratosphere could also be a source region where low H_2O and low O_3 can be found right above the tropical tropopause. Based on this correlation alone, these air masses suggest a tropical source influencing the top of the lowermost stratosphere over Florida, but the source region is not clearly identified.

CO_2 ranged from 371.5 to 374 ppmv during this regime. In the driest air masses (5 to 7 ppmv of H_2O), CO_2 varied between 373 and 373.8 ppmv. These values were found in the tropics (troposphere and stratosphere) as well as in the extratropical troposphere. Convective air from the extratropics would typically bring more than 7 ppmv of H_2O into the stratosphere. This leaves the tropics as the most likely source region. The range of the observations as well as the range of values in the tropical source regions shown in Table 2 cannot clearly differentiate UTT air from air coming from tropical lower stratosphere based on CO_2. The wettest air masses contained higher CO_2. This observation is consistent with a tropospheric source as we saw in regime 1 and 2; however, the variability of surface CO_2 inhibits constraining the origin of the tropospheric source.

NO_y ranged from 400 to 1400 pptv, which was the lowest range observed during the month. Air masses with the highest values of NO_y (1000 to 1400 pptv) contained between 8 and 13 ppmv of H_2O. These air masses can potentially come from the extratropical troposphere or from the UTT (B or C from Fig. 1) based on the values reported in Table 2. If we take a look at the NO-H_2O correlation, we immediately see that this high NO_y was not driven by recent convection that produced NO. This does not rule out the possibility of air that was influenced by convection a week prior to our detection over Florida where any NO that might have formed would have been converted to NO_y. These air masses might not be pure stratospheric nor pure tropospheric in character since H_2O is high to be pure stratospheric and NO_y is too high to be pure tropospheric. The composition of these air masses based on these two tracers suggest that they might be the result of mixing of stratospheric and tropospheric air instead. The driest air masses contained between 5 and 7 ppmv of H_2O and less than 500 pptv of NO_y. These air masses can come from the UTT (the H_2O mixing ratios are too low for a tropospheric source such as A(2) or B from Fig. 1) or the tropical lower stratosphere. Measurements during the various campaigns reported in Table 1 show that air in the tropical lower stratosphere has more than 500 pptv of NO_y. Measurements in the overworld between 12°N and 27°N during CRYSTAL-FACE actually show minimum values of NO_y of 600 pptv. Thus, the CRYSTAL-FACE measurements suggest that descent from the overworld (D from Fig. 1) was not the transport pathway, because the air would have had to carry more NO_y than what was observed.

Similar to regime 1, NO is mostly constant throughout the lowermost stratosphere during this regime. In the driest air masses (5-7 ppmv of H_2O), NO was also the lowest (around 150 pptv). This low NO along with the lowest NO_y observed during the entire month are consistent with the chemical composition of air masses coming from the UTT (C from Fig. 1). In the wettest air masses, NO mixing ratios almost doubled, but they still remained below 320 pptv. The low NO mixing ratios during this regime suggest that air could have come from any pathway except convection that was less than a week old.

During this regime, CO varied between 36 and 70 ppbv. The driest air masses found above the 375 K isentrope contained CO between 50 and 57 ppbv. These values are also consistent with a UTT source and exclude the tropical lower stratosphere as a possible source according to Table 2. The rest of the air masses in this region show a positive correlation between CO and H_2O, with the lowest mixing ratios for both tracers found below 375 K and the highest mixing ratios found near the tropopause. The lowest mixing ratios of CO suggest the presence of a stratospheric source. From this correlation alone, the origin of the stratospheric source is unclear. Air masses that contained the highest mixing ratios of H_2O and CO were of tropospheric origin. According to Table 2, the CO values fall within the range observed in the UTT. However, convective values of CO are so variable that we cannot exclude old convective air (A(2) from Fig. 1) as another source.

Lastly, we examine the CH_4-H_2O correlation during this regime. CH_4 mixing ratios ranged from 1720 to 1800 ppbv during this period. In the driest air masses, CH_4 varied between 1760 and 1790 ppbv. A combination of these two tracer ranges is not inconsistent with a tropical source. Because of the variability of CH_4 near the surface, this tracer

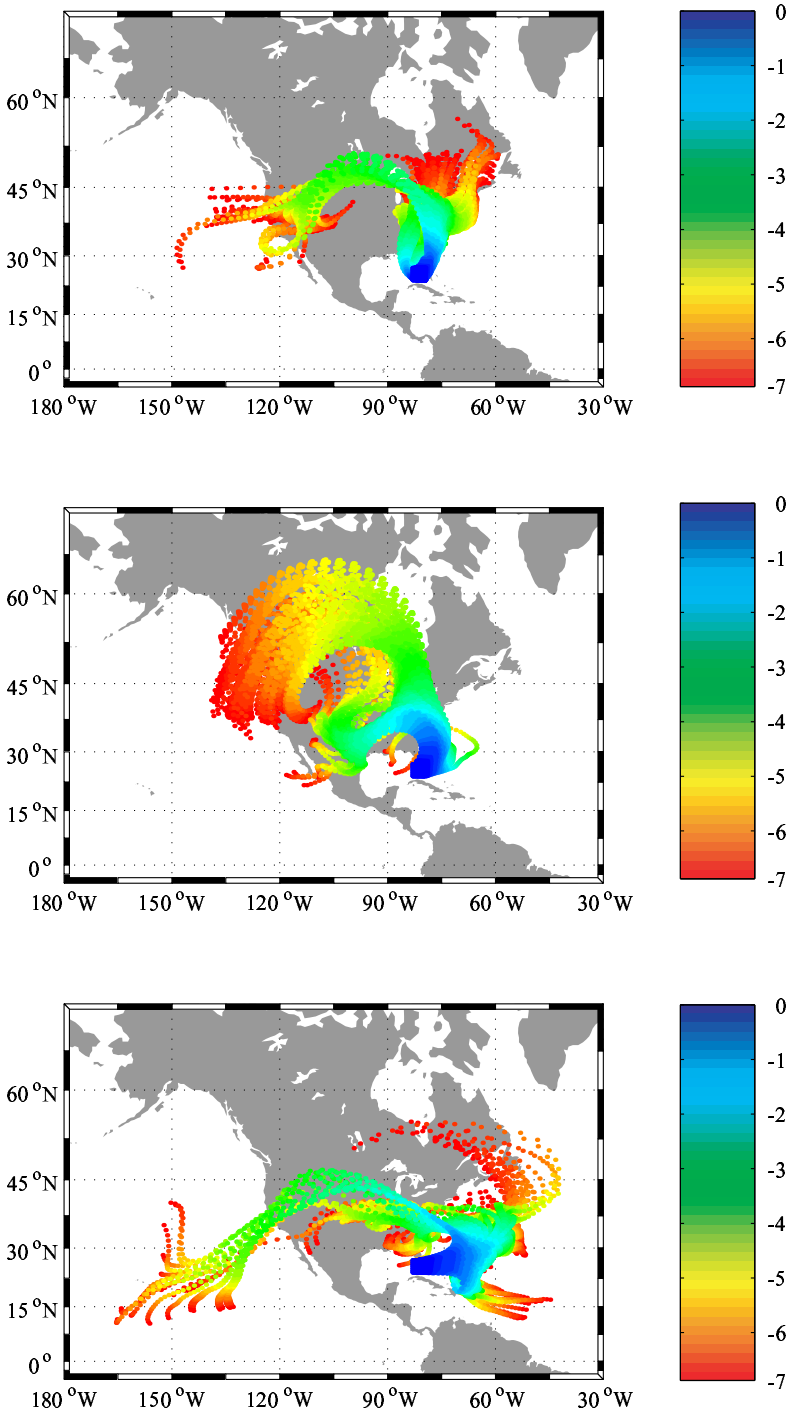

Figure 4. Horizontal plots of 7-day backward trajectories calculated using the FABtraj model. The top panel was initialized on July 7, 2002 (regime 1), the middle panel was initialized on July 19, 2002 (regime 2), and the bottom panel was initialized on July 28, 2002 (regime 3). The colors represent the number of days back in time as shown by the scale on the right.

alone cannot constrain the latitudinal origin of these air masses. During this regime, CH_4 values throughout the region were very close to surface values, which implies that a large fraction of the air in the lowermost stratosphere over Florida was of tropospheric origin. The stratospheric component characterized by low CH_4 and low H_2O that was observed during regime 2 is not observed during regime 3.

The combined information obtained from all the tracer-H_2O correlations during regime 3 allow us to come to the following conclusions. The following pathways left a signature of the source region in the lowersmost stratosphere over Florida: convection (high H_2O, lower O_3, high CO_2, and high CH_4 as seen in Figure 3), and poleward transport of UTT air (low H_2O, low O_3, low NO_y, low NO, high CO_2, and high CH_4). Air masses with more than 10 ppmv of H_2O were found below 370 K or the bottom 600 m of a 1.5-km deep lowermost stratosphere. The origin of the stratospheric source (O_3 and NO_y levels higher than tropospheric values) was not clearly identified (A(1) versus D from Fig. 1). When plotting vertical profiles of O_3, NO and NO_y

in the lowermost stratosphere over Florida (not shown), we see a discontinuity in the mixing ratios at 375 K suggesting that air masses above and below this break come from different source regions as reflected in their different chemical composition. If poleward transport of UTT air is controlling the chemical composition of air only above 375 K, then it is difficult to imagine that tropical lower stratospheric air is influencing the region below 375 K without affecting the region above 375 K. Therefore, we hypothesize that the source of stratospheric air is still equatorward transport of high-latitude air, but because of the tropospheric signature the stratospheric signature is weak and it would only show in tracers where the stratospheric values are greater than the tropospheric values, namely O_3 and NO_y.

3.3. Trajectories

In order to examine the origin of the air over Florida based on meteorological conditions, we use the FABtraj model to calculate 7-day backward trajectories. These trajectories were calculated using an integration time step of 30 minutes. We started the trajectories on three arbitrary days, each one corresponding to one of the three regimes identified by the tracer analysis.

We initialized each trajectory by constructing a box from 24°N to 27°N, from 80°W to 83°W, and from 145 hPa to 105 hPa. Parcels are separated by 0.5° in both latitude and longitude, and by 10 hPa in altitude, which results in a box with dimensions of 400 km in latitude, 300 km in longitude, and 2 km in depth. The box contained a total of 245 air parcels. The selected flights are July 7^{th} for regime 1, July 19^{th} for regime 2, and July 28^{th} for regime 3.

The backward trajectories are shown in Figure 4 and they are color-coded by number of days back in time. In this figure we only plot the horizontal component of the backward trajectories. During regime 1, trajectories show some air parcels traveling south from eastern Canada along the eastern seaboard and other air parcels originating in the West Coast of the U.S., traveling eastward along the U.S.-Canada border, and finally southward towards Florida over the course of seven days. During regime 2, trajectories show air parcels originating along the West Coast of both the U.S. and Canada, traveling eastward and then southward towards Florida. Three to four days prior to reaching Florida, 66% of the air parcels spent time over the central U.S. where convection is strong and frequent during this time of the year. During regime 3, air masses reaching Florida were under the influence of a strong easterly flow a couple of days prior to their arrival to Florida and had origins ranging from Canada to the tropics, and from the Pacific to the Atlantic Ocean.

In addition to horizontal motion, the model allows us to track the vertical motion driven by the divergence of horizontal winds. Since our original box was set in pressure coordinates in the vertical, all air parcels have the same mass so they are all equally weighted within the entire box. We label each air parcel in the box as stratospheric if its isentropic potential vorticity obtained from the model run is greater than 3 potential vorticity units, or PVU (1 PVU $= 10^{-6}$ m^2 K s^{-1} kg^{-1}). We choose 3 PVU, because it was the closest (within 5 K) to the 360 K isentrope, which was where the local tropopause was found during CRYSTAL-FACE. Figure 5 shows the percent of the original mass that stayed in the stratosphere based on the PV criterion during the backward trajectory.

For the flight selected during regime 1, the model shows that the original box is 100% stratospheric in character (day 0) and that at most 15% of tropospheric air (day -7) mixed into the box since 85% of the air parcels retained a PV equal to or greater than 3. For the flight selected during regime 2, the model shows that the initial box has 7% tropospheric character (day 0). This condition is in agreement with in situ data that show that the tropopause was at higher altitudes during regime 2. Since the initial location of the box was held constant for all three runs, tropospheric air was therefore found in the lower part of the box during this flight. The tropospheric component is at its maximum (20%) 3 to 4 days prior to reaching Florida. This is coincident with the air parcels that detoured towards the central U.S. and were most likely influenced by convection. For the flight selected during regime 3, the model shows a contribution of 4% of tropospheric air on day 0 and over 40% seven days prior to the arrival of the air parcels to southern Florida. The tropospheric source for the trajectories initialized on July 19 (regime 2) appears to be continental convection according to backward trajectory calculations. For the trajectories initialized on July 28 (regime 3), a contribution of 17% of the total mass comes from air parcels that originated and stayed over the ocean throughout the calculation. This analysis using changes in the altitude of the air parcels is intended for qualitative purposes. Quantification using this approach is difficult, because the model does not account for small-scale processes such as convection and mixing.

The results presented in this section show that backward trajectory calculations are in qualitative agreement with the information provided by tracer analysis in both space (horizontal and vertical) and time.

3.4. Monsoon Circulation

The tracer-H_2O correlations and backward trajectory calculations examined thus far show consistency in the origin of the air sampled in the lowermost stratosphere during CRYSTAL-FACE. The large-scale circulation observed over Florida during this campaign has been attributed to the presence of an upper level anticyclone over North America [*Richard et al.*, 2003] as seen in the pattern of the trajectories shown in Figure 4. According to 21 years of rawinsonde data, this anticyclone is expected to develop as part of the monsoon circulation in this region [*Dunkerton*, 1995]. We investigate the influence of the monsoon on transport pathways in the stratosphere by examining the O_3-H_2O correlation during the CRYSTAL-FACE and STRAT campaigns.

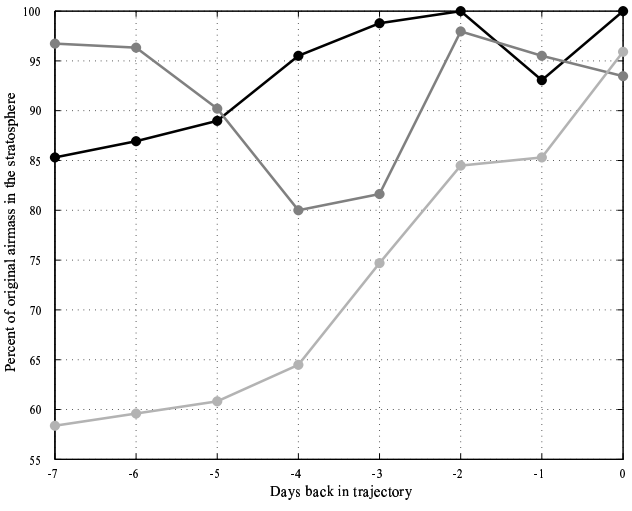

Figure 5. Percent stratospheric air based on air parcels with PV>3 PVU within the box advected back in time shown in Figure 4. The black line represents how the stratospheric component changed with time during the trajectory calculations initialized on July 7 (regime 1), the dark gray is for July 19 (regime 2), and the light gray is for July 28 (regime 3).

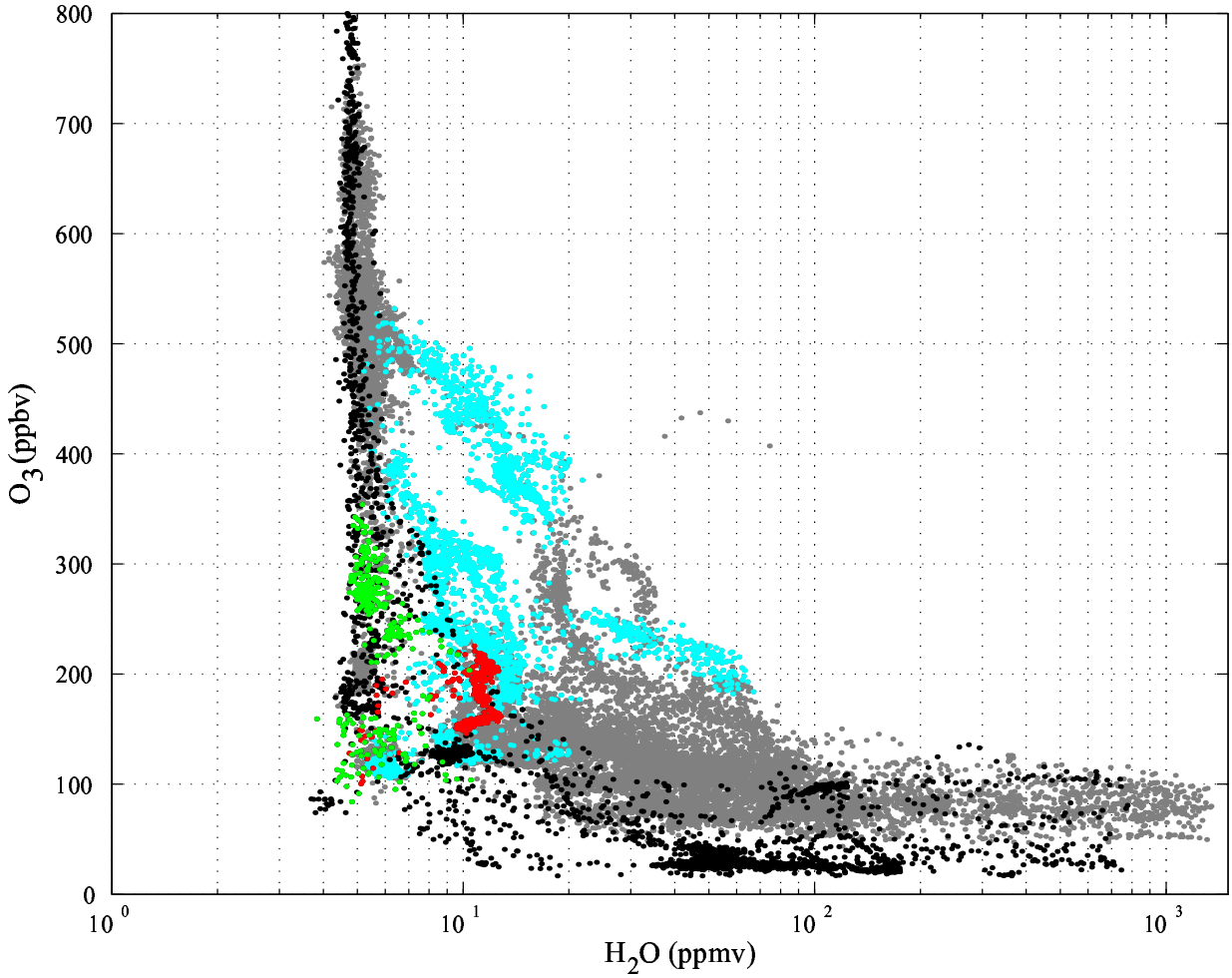

Figure 6. O_3-H_2O correlations for CRYSTAL-FACE and STRAT. The dark gray points correspond to data outside the lowermost stratosphere and the cyan points correspond to data within the lowermost stratosphere during CRYSTAL-FACE. The black points correspond to data outside the lowermost stratosphere during STRAT. The red points are lowermost stratospheric data over California and the green points are lowermost stratospheric data over Hawaii.

These two campaigns were chosen for several reasons: (i) they both collected in situ data in the lowermost stratosphere during the summer, (ii) they were located on opposite sides of the center of the monsoon, and (iii) they shared similar zonal boundaries (i.e., the jet stream on the north side, and the subtropical tropopause on the south side). During the summertime, the subtropical jet stream is weak due to a significant decrease in the temperature gradient between the tropics and the midlatitudes. This condition implies that transport across the tropopause in the subtropics is not inhibited as it is the case during the winter. During both missions, NCEP assimilated horizontal winds show the presence of only one jet stream located north of 40°N during STRAT, and between 45°N and 55°N during CRYSTAL-FACE.

The O_3-H_2O correlation for both campaigns is shown in Figure 6. Data both outside and within the local lowermost stratosphere are presented. When little mixing occurs between the troposphere and the stratosphere, this correlation has an 'L-shape'. The pure tropospheric air (horizontal part of the 'L') is characterized by low O_3 and varying amounts of H_2O (up to three orders of magnitude), whereas the pure stratospheric air (vertical part of the 'L') is characterized by low H_2O and varying amounts of O_3, which result from photochemical production in the stratosphere. Any departure from the pure profiles for each component implies mixing between these two regions. The point where both H_2O and O_3 are the lowest represents the tropopause, or transition between the troposphere and the stratosphere.

With this understanding in mind, Figure 6 reveals three interesting results. (i) Air in the lowermost stratosphere contained both more H_2O and more O_3 during CRYSTAL-FACE than during STRAT. (ii) The lowermost stratosphere over Florida is a more active region in terms of mixing stratospheric and tropospheric air compared to STRAT based on the greater number of mixing lines. (iii) During STRAT alone, we observe more mixing in the lowermost stratosphere over California than over Hawaii. These observations suggest a more dynamically active lowermost stratosphere over continental regions than over the ocean.

This tracer-tracer correlation is in agreement with the large-scale circulation inferred from rawinsonde data [*Dunkerton*, 1995] and modeling studies [*Chen*, 1995]. Air masses to the west of the anticyclone (e.g., STRAT) are under the influence of poleward transport of UTT air (low O_3), whereas air masses to the east of the anticyclone (e.g., CRYSTAL-FACE) are under the influence of equatorward transport of high-latitude stratospheric air instead (high O_3). In addition, the higher H_2O observed during CRYSTAL-FACE implies a stronger influence of tropospheric air in the stratosphere on the east side of the monsoon. This stronger influence is not only due to local but

also due to non-local convection that can influence the chemical composition of the air masses as they travel across the continent around the upper-level anticyclone.

4. Conclusions

We used tracer analysis and backward trajectory calculations to identify transport pathways that bring air into the subtropical lowermost stratosphere over Florida during July 2002. We identified three major transport pathways namely, equatorward transport of high-latitude stratospheric air, convection, and poleward transport of UTT air (A(1), A(2), B, and C from Fig. 1). The distinction between UTT air and air right above the tropical tropopause (i.e., air in the Tropical Transition Layer) is very hard to make based on the mixing ratios of tracers. Therefore, we cannot exclude the possibility of tropical air from 390 K for example arriving in Florida along with the UTT air; however, we can be more certain that air from higher potential temperatures (e.g., 400 - 420 K) in the tropics did not descend diabatically near or over Florida (D from Fig. 1), because the mixing ratios are significantly different that we would have identified them if air masses of this origin were present. Vertical profiles of tracers such as O_3 [*Richard et al.*, 2003] show a sharp gradient or discontinuity between the lowermost stratosphere and the overworld over Florida throughout the month of July. These observations corroborate that diabatic descent did not take place since the air masses in these two adjacent regions had very different O_3 mixing ratios.

Using an Eulerian approach and tracer correlations, we qualitatively identified each transport pathway and its region of influence throughout the month. Our analysis shows that the entire subtropical lowermost stratosphere (1.5 km in depth on average) was influenced by both high-latitude stratospheric air and by convective air throughout the campaign. The convective influence was not episodic, but rather persistent throughout the month. Even though H_2O mixing ratios in the lowermost stratosphere were as much as four times higher than stratospheric background levels, we found this region to be undersaturated for most of the month, and occasionally supersaturated. The tracers used in this study did not always allow us to distinguish the exact origin of the convective air (e.g., local, tropical, or extratropical) unless specific signatures like unusually high CO linked to high-latitude forest fires [*Jost et al.*, 2004] were present. Because strong and deep convective towers develop and can reach the stratosphere in a matter of hours, the use of short-lived species would have been of great advantage. The distinction between continental and maritime convection would also be useful and it could be achieved with the right choice of tracers. For instance, we could use formaldehyde and/or isoprene for the continental signature, and dimethyl sulfide and/or methyl iodide for the maritime signature. The shortest lived tracer available during CRYSTAL-FACE was NO, which has a lifetime of one week. Therefore, we could not distinguish convective air that was injected a few hours versus a few days (less than a week) prior to our measurement. This information would be useful to have in order to determine the origin, and thus the pathway of air that reaches a region of interest. Towards the end of the month, large-scale circulation patterns changed and affected the top 400 m of the lowermost stratosphere. At these altitudes, chemical tracers revealed the presence of UTT air over Florida.

Backward trajectory calculations showed that transport to Florida can be very fast (e.g., equatorward transport from Canada in 1 to 2 days, westerly transport from the West Coast to the east coast in 1 to 3 days) and very slow (poleward transport from the UTT in 6 to 7 days regardless of whether the air originated in the tropical Atlantic or the tropical Pacific).

Correlation plots using in situ measurements of O_3 and H_2O in the subtropics and midlatitudes show the longitudinally dependent transport pathways associated with the upper-level circulation near monsoon regions. *Richard et al.* [2003] identified a high-pressure system over the central U.S. for most of the month, which was suggested to be the driver for the equatorward transport of air towards Florida. If this is a persistent summertime feature as climatological data show, then this type of transport along with a threat of increasing convective activity in the future due to global warming can have a larger impact on the chemical composition and radiative balance of the lowermost stratosphere by not only adding H_2O but also polluted air from the boundary layer. Analogous to the stratospheric fountain, the role of bringing boundary layer air into the stratosphere as we saw during CRYSTAL-FACE might be specific to particular geographical regions. The chemistry of the stratosphere over specific geographical locations can then be more influenced by tropospheric air and can play a more important role in stratosphere-troposphere exchange than it has been thought before. Transport of more tropospheric air in these regions could further decrease the total column of ozone by both chemical and dynamical processes. Chemically by bringing constituents such as aerosols and water vapor at levels higher than the stratospheric background, which coupled with stratospheric cooling due to the radiative effect of increasing greenhouse gases such as CO_2, can lead to in situ chemical loss. Dynamically by transporting ozone-poor air into the stratosphere via pathways that do not simply redistribute the ozone within the column (e.g., local convection that transports air into the stratosphere above) but bring it from different geographical locations as *Jost et al.* [2004] showed.

In this study we identified that spatial and temporal coverage of the transport pathways that bring air into the subtropical lowermost stratosphere. Our next study will focus on quantifying the contribution of each pathway using a simple mixing model based on tracer profiles from different latitudinal origins.

Acknowledgments. We are very grateful to the WB-57 flight and ground crew as well as the CRYSTAL-FACE mission planners for their hard work in making this mission possible. We would like to thank the NOAA Climate Monitoring and Diagnostics Laboratory for providing surface measurements. J. R. Spackman provided useful comments on this manuscript. J. V. Pittman acknowledges the NASA Earth System Science Graduate Student Fellowship for their support during the course of this research project. This work was funded in part by the NASA Upper Atmospheric Research Program.

References

Boering, K. A., S. C. Wofsy, B. C. Daube, H. R. Schneider, M. Loewenstein, J. R. Podolske, and T. J. Conway (1996), Stratospheric mean ages and transport rates from observations of carbon dioxide and nitrous oxide, *Science*, *274*, 1340–1343.

Brasseur, G., and S. Solomon (1986), *Aeronomy of the Middle Atmosphere: Chemistry and Physics of the stratosphere and mesosphere*, Dordrecht, Boston, Mass.

Brewer, A. W. (1949), Evidence for a world circulation provided by measurements of helium and water vapor in the stratosphere, *Quart. J. Roy. Meteorol. Soc.*, *75*, 351–363.

Chen, P. (1995), Isentropic cross-tropopause mass-exchange in the extratropics, *J. Geophys. Res.*, *100*(D8), 16,661–16,673.

Cooper, O., C. Forster, D. Parrish, M. Trainer, E. Dunlea, T. Ryerson, G. Hbler, F. Fehsenfeld, D. Nicks, J. Holloway, J. de Gouw, C. Warneke, J. M. Roberts, F. Flocke, and J. Moody (2004), A case study of trans-pacific warm conveyor belt transport: The influence of merging airstreams on trace gas import to north america, *J. Geophys. Res.*, *109*(23), D23S09, doi:10.1029/2003JD004006.

Daube, B. C. J., K. A. Boering, A. E. Andrews, and S. C. Wofsy (2002), A high-precision fast-response airborne CO_2 analyzer for in situ sampling from the surface to the middle stratosphere, *J. Atmos. and Ocean Tech.*, *19*, 1532–1543.

Denning, R. F., S. L. Guidero, G. S. Parks, and B. L. Gary (1989), Instrument description of the airborne microwave temperature profiler, *J. Geophys. Res.*, *94*(D14), 16,757–16,765.

Dessler, A. E., E. J. Hintsa, E. M. Weinstock, J. G. Anderson, and K. R. Chan (1995), Mechanisms controlling water vapor in the lower stratosphere: "A tale of two stratospheres", *J. Geophys. Res.*, *100*(D11), 23,167–23,172.

Dethof, A., A. O'Neill, and J. Slingo (2000), Quantification of the isentropic mass transport across the dynamical tropopause, *J. Geophys. Res.*, *105*(D10), 12,279–12,293.

Dobson, G. M. B. (1956), Origin and distribution of the polyatomic molecules in the atmosphere, *Proc. R. Soc. London, Ser. A*, *236*, 187–193.

Dunkerton, T. J. (1995), Evidence of meridional motion in the summer lower stratosphere adjacent to monsoon regions, *J. Geophys. Res.*, *100*(D8), 16,675–16,688.

Hintsa, E. J., K. A. Boering, E. M. Weinstock, J. G. Anderson, B. L. Gary, L. Pfister, B. C. Daube, S. C. Wofsy, M. Loewenstein, J. R. Podolske, J. J. Margitan, and T. P. Bui (1998), Troposphere-to-stratosphere transport in the lowermost stratosphere from measurements of H_2O, CO_2, N_2O and O_3, *Geophys. Res. Lett.*, *25*(14), 2655–2658.

Hoskins, B. J. (1991), Towards a PV-Theta view of the general circulation, *Tellus Ser. A and B*, *43*(4), 27–35.

Jost, H. J., K. Drdla, A. Stohl, L. Pfister, M. Loewenstein, J. P. Lopez, P. K. Hudson, D. M. Murphy, D. J. Cziczo, M. Fromm, T. P. Bui, J. Dean-Day, C. Gerbig, M. J. Mahoney, E. C. Richard, N. Spichtinger, J. V. Pittman, E. M. Weinstock, J. C. Wilson, and I. Xueref (2004), In situ observations of mid-latitude forest fire plumes deep in the stratosphere, *Geophys. Res. Lett.*, *31*(11), L11,101, doi:10.1029/2003GL019253.

Loewenstein, M., H. Jost, J. Grose, J. Eilers, D. Lynch, S. Jensen, and J. Marmie (2002), Argus: A new instrument for the measurement of the stratospheric dynamical tracers, N_2O and CH_4, *Spectrochim. Acta A*, *58*(11), 2329–2345.

Logan, J. A., I. A. Megretskaia, A. J. Miller, G. C. Tiao, D. Choi, L. Zhang, R. S. Stolarski, G. J. Labow, S. M. Hollandsworth, G. E. Bodeker, H. Claude, D. D. Muer, J. B. Kerr, D. W. Tarasick, S. J. Oltmans, B. Johnson, F. Schmidlin, J. Staehelin, P. Viatte, and O. Uchino (1999), Trends in the vertical distribution of ozone: A comparison of two analyses of ozonesonde data, *J. Geophys. Res.*, *104*(D21), 26,373–26,399.

Plumb, R. A. (2002), Stratospheric transport, *J. Meteorol. Soc. Jpn.*, *80*(4B), 793–809.

Poulida, O., R. R. Dickerson, and A. Heymsfield (1996), Stratosphere-troposphere exchange in a midlatitude mesoscale convective complex, *J. Geophys. Res.*, *101*(D3), 6823–6836.

Prados, A. I., G. E. Nedoluha, R. M. Bevilacqua, D. R. Allen, K. W. Hoppel, and A. Marenco (2003), POAM III ozone in the upper troposphere and lowermost stratosphere: Seasonal variability and comparisons to aircraft observations, *J. Geophys. Res.*, *108*(D7), 4218, doi:10.1029/2002JD002819.

Proffitt, M. H., and R. J. McLaughlin (1983), Fast-response dual-beam UV-absorption ozone photometer suitable for use on stratospheric balloons, *Rev. Sci. Instrum.*, *54*(12), 1719–1728.

Richard, E. C., K. K. Kelly, R. H. Winkler, R. Wilson, T. L. Thompson, R. J. McLaughlin, A. L. Schmeltekopf, and A. F. Tuck (2002), A fast-response near-infrared tunable diode laser absorption spectrometer for in situ measurements of CH_4 in the upper troposphere and lower stratosphere, *Appl. Phys. B*, *75*, 183–194.

Richard, E. C., K. C. Aikin, E. A. Ray, K. H. Rosenlof, T. L. Thompson, A. Weinheimer, D. Montzka, D. Knapp, B. Ridley, and A. Gettelman (2003), Large-scale equatorward transport of ozone in the subtropical lower stratosphere, *J. Geophys. Res.*, *108*(23), 4714, doi:10.1029/2003JD003884.

Ridley, B. A., J. G. Walega, J. E. Dye, and F. E. Grahek (1994), Distributions of NO, NO_x, NO_y, and O_3 to 12-km altitude during the summer monsoon season over New Mexico, *J. Geophys. Res.*, *99*(D12), 25,519–25,534.

Ridley, B. A., J. E. Dye, J. G. Walega, J. Zheng, F. E. Grahek, and W. Rison (1996), On the production of active nitrogen by thunderstorms over New Mexico, *J. Geophys. Res.*, *101*(D15), 20,985–21,005.

Ridley, B. A., E. Atlas, H. Selkirk, L. Pfister, D. M. J. Walega, S. Donnelly, V. Stroud, E. Richard, K. Kelly, A. Tuck, T. Thompson, J. Reeves, D. Baumgardner, W. T. Rawlins, M. Mahoney, R. Herman, R. Friedl, F. M. F, E. Ray, and J. Elkins (2004), Convective transport of reactive constituents to the tropical and rigid-latitude tropopause region: I. Observations, *Atmos. Env.*, *38*(9), 1259–1274.

Rosenlof, K. H. (1995), Seasonal cycle of the residual mean meridional circulation in the stratosphere, *J. Geophys. Res.*, *100*(D3), 5173–5191.

Stohl, A., P. Bonasoni, P. Cristofanelli, W. Collins, J. Feichter, A. Frank, C. Forster, E. Gerasopoulos, H. Gaggeler, P. James, T. Kentarchos, H. Kromp-Kolb, B. Kruger, C. Land, J. Meloen, A. Papayannis, A. Priller, P. Seibert, M. Sprenger, G. J. Roelofs, H. E. Scheel, C. Schnabel, p. Siegmund, L. Tobler, T. Trickl, H. Wernli, V. Wirth, P. Zanis, and C. Zerefos (2003), Stratosphere-troposphere exchange: A review, and what we have learned from STACCATO, *J. Geophys. Res.*, *108*(D12), 8516, doi:10.1029/2002JD002490.

Thompson, T. L., and K. H. Rosenlof (2003), Accuracy and precision of the NOAA Aeronomy Laboratory pressure temperature instrument on the NASA WB-57F, paper presented at CRYSTAL-FACE Science Team Meeting, NASA, Salt Lake City, UT.

Vaughan, G., and C. Timmis (1998), Transport of near-tropopause air into the lower midlatitude stratosphere, *Quart. J. Roy. Meteorol. Soc.*, *124*(549), 1559–1578.

Weinstock, E. M., E. J. Hintsa, A. E. Dessler, J. F. Oliver, N. L. Hazen, J. N. Demusz, N. T. Allen, L. B. Lapson, and J. G. Anderson (1994), New fast-response photofragment fluorescence hygrometer for use on the NASA ER-2 and the perseus remotely piloted aircraft, *Rev. Sci. Instr.*, *65*(11), 3544–3554.

WMO (2003), *Scientific assessment of Ozone depletion: 2002*, World Meteorological Organization, Global Ozone Research and Monitoring Project- Report No. 47, Geneva, Switzerland.

Xueref, I., C. Gerbig, A. Fridlind, J. C. Lin, S. Wofsy, B. C. Daube, J. B. Smith, D. Sayres, J. Vellovic, D. G. Baumgardner, A. Ackerman, E. Weinstock, A. E. Andrews, E. W. Gottlieb, and J. G. Anderson (2004), Coupling a receptor-oriented framework for tracer distributions with a cloud resolving model to study transport in deep convective clouds: application to the CRYSTAL FACE campaign, *Geophys. Res. Lett.*, *31*(14), L14,106, doi:10.1029/2004GL019811.

Jasna V. Pittman, Department of Earth and Planetary Sciences, Harvard University, Cambridge, MA 02138, USA. (vellovic@huarp.harvard.edu)

Quantifying the Impact of the North American Monsoon and Deep Midlatitude Convection on the Subtropical Lowermost Stratosphere Using In Situ Measurements on the NASA WB57 During the CRYSTAL FACE Campaign

E. M. Weinstock[1], J. V. Pittman[2], D. S. Sayres[2], J. B. Smith[2], J. G. Anderson[1], S. C. Wofsy[2], I. Xueref[2], C. Gerbig[2], B. C. Daube[2], E. C. Richard[3], B. A. Ridley[4], A. Weinheimer[4], H.-J. Jost[5], J. P. Lopez[5], M. Loewenstein[5], L. Pfister[5], and T. L. Thompson[3]

[1]Division of Engineering and Applied Sciences, Harvard University, Cambridge, Massachusetts, USA.
[2]Department of Earth and Planetary Sciences, Harvard University, Cambridge, Massachusetts, USA.
[3]Aeoronomy Laboratory, National Oceanic and Atmospheric Administration, Boulder, Colorado, USA.
[4]Atmospheric Chemistry Division, National Center for Atmospheric Research, Boulder, Colorado, USA.
[5]NASA Ames Research Center, Moffett Field, California, USA.

Abstract. The composition of the lowermost stratosphere can be highly variable both in spatial and temporal coordinates in that depending upon the relative strengths of various transport pathways, from the TTL through isentropic transport, from all latitudes of the stratosphere through diabatic descent and isentropic transport, and from the troposphere through convection serving as the possible source regions. Back trajectory calculations clearly indicate that much of the air sampled during the Cirrus Regional Study of Tropical Anvils and Cirrus Layers-Florida Area Cirrus Experiment (CRYSTAL FACE) had been entrained in the anticyclonic jet associated with the North American monsoon. In situ measurements made in the lowermost stratosphere over Florida during the mission during July 2001 clearly illustrate the impact of equatorward flow around the monsoon, with ozone mixing ratios of between 300–600 ppbv serving as the most obvious indicator. However, this flow also carries along with older stratospheric air the distinct signature of deep midlatitude convection as well and it is important to establish a framework to quantify the convective contribution, as well that from other source regions. We use simultaneous in situ measurements of water vapor, ozone, NOy, carbon dioxide, and carbon monoxide in the framework of a simple box model to quantify the composition of the air sampled in the lowermost stratosphere during the mission based on tracer mixing ratios ascribed to these source regions. The results show that in the summer, convection has a significant impact on the composition of air in the lowermost stratosphere, being the dominant source of water vapor up to the 380 K isentrope, and an important source of NOx through lightning, which is reflected in our data by elevated NOy. The implications of these results extend from additional homogeneous ozone loss from NOx injection, to the potential for (additional) heterogeneous ozone loss resulting from the increased frequency and lifetime of cirrus above the local tropopause, to air with increased water vapor that as part of the equatorward flow associated with the North American monsoon can become part of the general circulation.

Introduction

A key societal objective for Earth science research is to provide credible forecasts defining trends in UV radiation dosage to populated areas globally. This objective of forecasting requires a rigorous understanding not only of the mechanisms that control ozone loss in the stratosphere, but also the processes that control aerosol formation, cirrus cloud formation, stratosphere/troposphere exchange and the photochemical mechanisms controlling ozone formation and loss in the troposphere. Ultimately, elucidating the critical link between UV dosage and climate change requires an understanding of the coupling of dynamics, chemistry, and radiation especially within the tropical tropopause layer, and the midlatitude upper troposphere and lower stratosphere. The lowermost stratosphere, the region in the extra-tropics bounded from above by the isentrope corresponding to the tropical tropopause, typically 380–390 K, and from below by the local tropopause, is a critical part of this domain. This is especially true because the analysis of ozonesondes in northern midlatitudes [Logan et al., 1999] has shown a decrease of about 1%/year during the 1990s, with the maximum % ozone loss occurring in the lowermost stratosphere. A conclusion of the 2002 Scientific Assessment of Ozone Depletion [WMO, 2003] is that

the vertical, latitudinal, and seasonal characteristics of changes in midlatitude ozone are broadly consistent with the understanding that halogens are the primary cause, in line with similar conclusions from the 1998 Assessment. It also states that atmospheric dynamics has contributed to this and that chemical and dynamical effects are coupled and cannot be assessed in isolation.

The potential of a direct dynamical component to an ozone trend can be easily imagined when one considers the range of ozone mixing ratios in the different regions that potentially supply the lowermost stratosphere, where a significant fraction of the ozone column resides. Hudson et al. [2003] use column ozone data from the Total Ozone Mapping Spectrometer (TOMS) to illustrate that there are different meteorological regimes bounded by the position of the subtropical and polar fronts that have characteristic ozone profiles. The statistics of the position of these fronts clearly impact not only average stratospheric ozone column amounts but profile averages as well.

There is also a postulated chemical component, which has as well an indirect dynamical component associated with it. Using measurements of ClO with inferred BrO near the polar tropopause Thornton et al. [2003] calculation ozone destruction rates of about 1 ppbv/day, thus accounting for destruction of about 10% of the ozone near 12 km north of 55N latitude. The authors suggest that this level of ozone loss can explain the ozone trend observed in winter and spring. Similarly, the UNEP report continues to invoke the possibility of heterogeneous ozone loss at the surface of ice particles in cirrus clouds in this region. However, for these clouds to have a significant impact on ozone, they need to be above the local tropopause [Smith et al., 2002]. Accordingly, interest in cirrus cloud climatology extends beyond its radiative impact to the question of heterogeneous ozone depletion. Cirrus cloud formation and lifetime depends on background water vapor mixing ratios, and in the lowermost stratosphere the relative humidity of the air is strongly dependent upon the extent to which the air has tropospheric character versus stratospheric character. Accordingly, understanding the makeup and origin of this air and what controls its tracer characteristics should be very important for cirrus cloud lifetimes.

As has been previously noted [Poulida 1996; Jost et al., 2004] midlatitude convection can transport organic pollutants and water into the lowermost stratosphere and on occasion extends to and beyond the 380K isentrope. Equatorward isentropic transport, influenced by monsoon circulation in both hemispheres [Dunkerton, 1995; Pittman et al., 2004, Bannister et al., 2004] provides a viable although poorly documented pathway for lowermost stratospheric air, perturbed by midlatitude convection, to enter the upper tropical troposphere (UTT) and subsequently enter the general circulation. Quantitatively characterizing this air and its source regions is important. Accordingly, finding ways to quantify the contribution of convection to middleworld air, especially during northern latitude summer is important both to increase our understanding of the control of humidity in this region as well as the potential for increasing the humidity of the lower tropical stratosphere in summer.

In situ studies of the composition of the lowermost stratosphere and the contributing transport pathways have been provided mainly by tracer measurements made on research aircraft. Measurements on the NASA ER2 during the Stratospheric Photochemistry, Aerosols, and Dynamics Expedition (SPADE) in 1993 [Hintsa et al., 1994; Dessler et al., 1995] and the Stratospheric Tracers of Atmospheric Transport (STRAT) campaign from October 1995 to December 1996 [Hintsa et al., 1998] all provided examples of isentropic mixing of air from the upper troposphere into the subtropical and midlatitude lowermost stratosphere. Additionally, as part of the Observation in the Middle Stratosphere (OMS) balloon program Ray et al. [1999] used analysis of long-lived tracers from balloon-borne instruments in mid- and high latitudes in 1996, 1997, and 1998 to quantitatively measure the percentage of stratospheric and tropospheric air in the lowermost stratosphere. The general thrust of these measurements is that there is a seasonal dependence to the relative amounts of tropospheric and lower stratospheric air in the lowermost stratosphere, where poleward isentropic transport competes with descent from the overworld.

While these studies have focused on differentiating a tropospheric component of lowermost stratosphere air from a stratospheric component, they have not looked closely at the stratospheric component. For example, Dessler et al. [1995] focused on water vapor profiles in the lowermost stratosphere taken over NASA Ames, CA (37.4°N, 122.1°W) during the Stratospheric Photochemistry, Aerosols, and Dynamics Expedition (SPADE) to illustrate a significant fraction of tropospheric air above

the local tropopause. He did not examine the corresponding ozone, carbon dioxide, and nitrous oxide tracer-tracer correlations that demonstrate variability in the stratospheric component of the air mass and the reason for that variability. In fact, Newman et al. [1996] demonstrate that laminae observed above 400 K during SPADE over Ames result from the breakup of the polar vortex. The degree to which equatorward flow in the lowermost stratosphere providing ozone enhancement correlates with observation of vortex filaments above has not been explored in depth. However, Figure 1 of Newman et al. [1996] does illustrate evidence of that correlation, with the strongest filament centered at about 460 K, and smaller ones centered at 410 K, 380 K, and 360 K.

A series of aircraft missions were carried out in Europe between November 2001 and July 2003 to study dynamics and mixing in the midlatitude tropopause region. The SPURT (SPURenstofftransport in der Tropopausenregion, Trace Gas Transport in the Tropopause Region) campaign, studied the spatial and seasonal distribution of tracers in the UT/LS region. The results of the airborne in situ observations during the SPURT project illustrate that tropopause to stratosphere transport and subsequent mixing significantly alter the chemical composition in a narrow band above the local tropopause, and the width of that band exhibits a seasonal dependence.

The CRYSTAL FACE (CF) campaign took place during the month of July in Key West, Florida (23°N latitude, 84°W longitude), during which the NASA WB57F aircraft flew 12 science flights in addition to the ferry fight from Houston. While most of the flights focused on the study of cirrus in the upper troposphere, flight trajectories often included climbs into the lower stratosphere, up to 440 K. Starting with the ferry flight from Houston to Key West, and continuing throughout much of July, tracer data in the lower stratosphere, from 360 K up to 410 K, show strong evidence of equatorward transport of air [Richard et al., 2003]. Richard et al. [2003] additionally showed that anticyclonic flow, consistent with the North American monsoon, was responsible for this transport, and the 3-D modeling study on July 3, 2002 using the MOZART chemical-transport model, version 3 [Brasseur et al., 1998] driven by ECMWF analyzed meteorological fields. The model shows a large enhanced region of ozone from about 360 to 410 K over the southeastern US. The observation of increased ozone mixing ratios in the middleworld resulting from significant equatorward flow illustrates the potential seasonal and meridional ozone variability resulting from transport alone, and its correlation with monsoon flow suggests a potential cause and effect relationship between climate and reported trends in midlatitude ozone depletion. Dunkerton [1995] used radiosonde data and European Center for Medium-Range Weather Forecasts analyses to study meridional circulation in association with the North American monsoon. He found that horizontal circulations do penetrate the lower stratosphere and southward flow over eastern North America is weaker than its poleward counterpart over western North America. Additionally, using a semi-Lagrangian model and ECMWF analysis, Chen [1995] shows that active cross tropopause isentropic transport occurs in the northern hemisphere summer and is mainly associated with the Mexican monsoon. Accordingly, understanding the impact of the monsoon on measured ozone values requires addressing the tropospheric content of these lower stratospheric air masses along with the strength of the equatorward flux.

While the ozonesonde network has contributed significant climatological information on the middleworld, and there are sites in the US and Canada that have provided weekly ozonesondes in North America during the last few decades, without additional simultaneous tracer data, analysis of that ozone dataset has not indicated a clear pattern of equatorward transport in the 340–400 K region. The extent of in situ ozone data with simultaneous measurements of different tracers in this region is limited, much of it obtained during the Stratospheric Tracers of Atmospheric Transport (STRAT) campaign from October 1995–December 1996. The data, taken primarily in midlatitudes off the western coast of the US and in the subtropics near Hawaii, typically illustrate rapid poleward transport of tropical air in the TTL, especially in the winter and early spring. Analysis of data taken during the Photochemistry of Ozone Loss in the Arctic region in Summer (POLARIS) in 1997 also showed no evidence of equatorward transport.

In part I of these studies, Pittman et al. [2004] have used tracer-tracer correlations and 3-D back trajectory calculations [Cooper et al., 2004] to identify three major source regions that supply air to the subtropical lowermost stratosphere as observed during CF. The back trajectories show that air coming out

of the tropical tropopause layer (TTL) as part of the monsoonal circulation can entrain stratospheric air with a range of median ages, as well as convective air from both northern midlatitudes and in the subtropics. The measured tracer-tracer correlations reflect the changing circulation patterns throughout the month of July illustrated in Figure 6 of Pittman et al.

We focus here on using the stratospheric and upper tropospheric tracer measurements as a means of quantifying the observed fraction of air from the above source regions. The analysis can then be coupled with chemical transport models that should quantitatively relate measured tracer mixing ratios to back trajectories. Transport of air throughout this region is generally described by a Holton-type diagram. [Holton, 1995]. We illustrate a version of this type of diagram in Figure 1, where we focus on a section of the lowermost stratosphere within the rectangle to represent the air sampled during CF over Florida. Transport of air into the rectangle is represented by the heavy black arrows, typically resulting in a mixture of stratospheric air (path 1) and tropospheric air (path 2). Evidence for these transport paths have been mainly provided by in situ tracer measurements made on the NASA ER2 aircraft during the Stratospheric Photochemistry, Aerosols, and Dynamics Expedition (SPADE) in 1993 [Hintsa et al., 1994; Boering et al., 1995; Dessler et al., 1995; Boering et al., 1996] and the Stratospheric Tracers of Atmospheric Transport (STRAT) campaign from October 1995–December 1996 [Hintsa et al., 1998]. Returning to Figure 1, we note the potential of two additional transport pathways into the middleworld region circumscribed by the rectangle. The vertical arrows represent convection, which typically transports air into the upper troposphere, and on occasion into the lowermost stratosphere. The horizontal arrow, pointing equatorward, represents the potential for isentropic transport of northern latitude air to the midlatitudes, the subtropics, and potentially into the tropics. This pathway has been postulated before as a possible means of exporting ozone poor air descending out of the arctic vortex to midlatitudes in spring. [Spackman et al., 2004]. However, during the SOLVE campaign from January to March 2000, no evidence of this was observed in the tracer data taken above 350 K on the ER2.

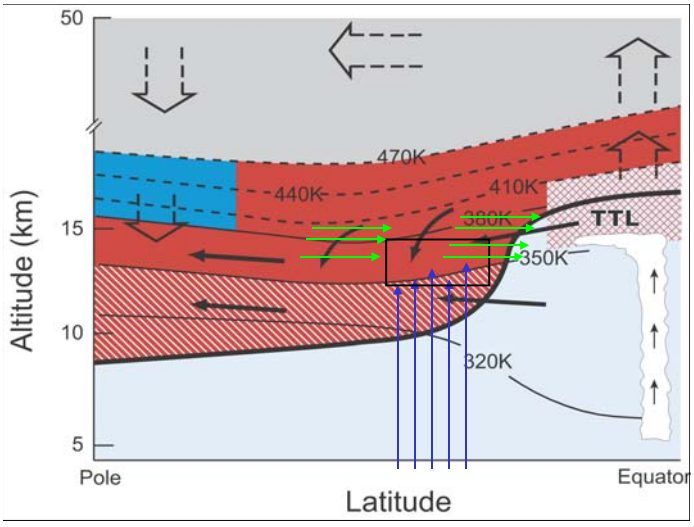

Figure 1. A plot of isentropic surfaces as a function of latitude and altitude. Transport into a section of the lowermost stratosphere within the rectangle illustrated here, is represented by the heavy black arrows, typically resulting in a mixture of stratospheric air (path 1) and tropospheric air (path 2). The horizontal green arrows, pointing equatorward, represent the potential for isentropic transport of northern latitude air to the midlatitudes, and even into the tropics (path 3). The vertical arrows represent convection, which typically transports air into the upper troposphere, and on occasion into the lowermost stratosphere (path 4).

Being two-dimensional, this figure has the disadvantage of not illustrating the continuity of transport between some of the pathways connected by longitudinal flow. As we discuss in detail later, back trajectories indicate that much of the air sampled in the lowermost stratosphere during CF came from northern midlatitudes as part of anticyclonic flow around the North American monsoon. [Richard et al., 2003]. What these 7–10 day trajectories do not indicate is what fraction of that air originated in the upper tropical troposphere (TTL), as would be expected as air is traveling poleward along the western side of the anticyclone. Accordingly, this flow pattern provides an opportunity for air in the northern midlatitude lower stratosphere to be mixed with UTT air before heading equatorward. Additionally, Figure 1 includes a convective contribution to lowermost stratospheric air from local convection over Florida. It does not explicitly include, however, midlatitude convection along the back trajectory that not

only is a source of boundary layer air to the lowermost stratosphere but also potentially serves as a turbulent mixer that enhances the entrainment of local stratospheric air into the monsoonal flow.

In the next section we provide examples of in situ tracer data from CF that we compare with data from the STRAT and POLARIS missions to illustrate the character of the air mass. We follow with a description of the mixing model used to quantify the contribution of each transport pathway. This section also details how the tracer composition of the air masses from each of the source regions is determined. We use data from the Houston to Key West ferry flight on June 29, 2002, during CF to quantify the fractions of air originating from each of the designated source regions. We have chosen this flight because it provides for analysis air masses with large variations of tracer mixing ratios between 350–390 K. We explore, as well, sensitivity of the model to the set of tracers used and to uncertainties in the source region tracer profiles. Finally, we fit to a merged dataset, allowing a determination of the average contributions of convective, UTT, and stratosphere air to the lowermost stratosphere over Florida during the three regimes identified in Pittman et al. [2004].

CF tracer data

Before investigating these data, however, it is useful to provide some context of what you might expect to see based on previous in situ measurements in this region. In Figures 2 and 3 we present tracer-tracer correlations taken during the summer, respectively, during the STRAT and POLARIS campaigns. Superimposed on each of the tracer plots is the comparable profile for the 20020703 flight that most clearly illustrates equatorward transport in the lowermost stratosphere. Starting with STRAT data, taken in July 1996 on NASA ER2 flights from Ames Research Center (37°N, 122°W), we see in panel (a) ozone plotted versus theta with ozone ranging from about 50–100 ppbv near the tropopause to about 200 ppbv at 380 K. In contrast, ozone in the middleworld is much higher during the 20020703 CF flight, increasing to 500 ppbv at 380 K. The implication here is that a significant fraction of the sampled air mass has been in the stratosphere for a long enough period of time to allow for increased photochemical production of ozone. If we look at panel (b), a plot of water vapor versus theta, we see that in the same region the profiles have varying degrees of water throughout the region, with only the 19960718 STRAT profile being indicative of much less tropospheric content than in the other flights. Panel (c) illustrates the clear difference in the character of the air between STRAT and the representative CF flight. From this plot of water vapor versus ozone, it appears that the air might be a simple mixture of stratospheric and tropospheric air, with the data points falling on a mixing line between stratospheric air with 550 ppbv ozone and about 5 ppmv water vapor and tropospheric air with 50 ppbv ozone and 60 ppmv water vapor. We include for reference a plot of CO_2 versus theta in panel (d), and CO_2 versus ozone in panel (e). For these plots, CO_2 during STRAT was increased by 9.5 ppmv to account for the secular trend in CO_2 between 1996 and 2002 of approximately 1.5 ppmv/year [Conway et al., 2003]. These plots similarly show the “older” stratospheric air during the 20020703 flight.

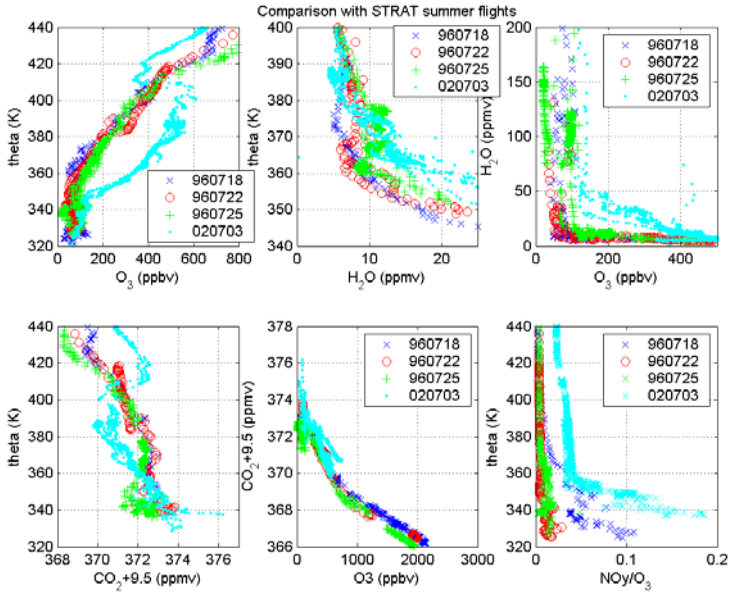

Figure 2. Tracer plots for the 20020703 flight during CF compared with summer tracer profiles measured during the STRAT campaign from NASA Ames Research Center, CA (37°N, 122°W). The STRAT CO_2 profiles are adjusted to account for the secular trend in stratospheric CO_2.

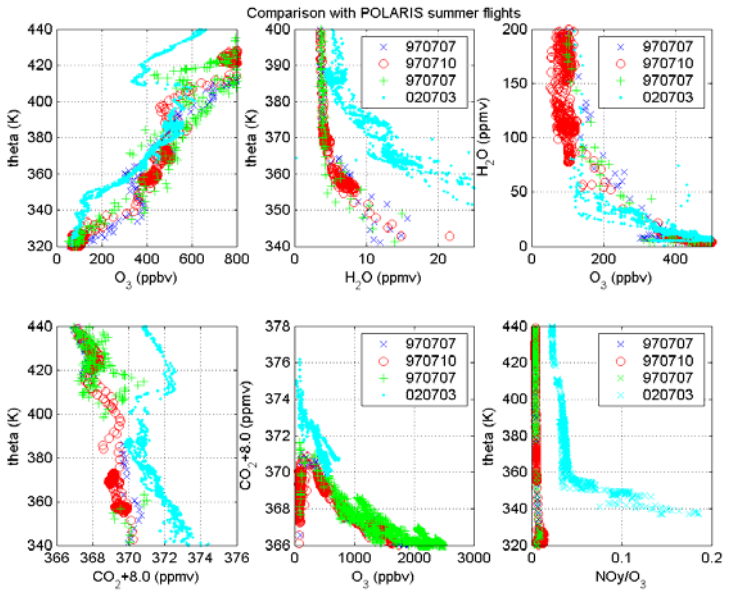

Figure 3. As in Figure 2, but comparing the 20020703 flight with summer profiles from the POLARIS mission out of Fairbanks, Alaska (65N, 148W).

Turning to the POLARIS data presented in Figure 3, we see a totally different but yet complementary picture. The middleworld air in the POLARIS flights is older, accounting for higher ozone, as shown in panel (a), while panel (b) illustrates that water vapor is significantly lower, illustrating that this air is virtually all stratospheric in character, with only slight tropospheric character increasingly influencing the profile with decreasing theta. Panel (e) illustrates the relatively tight correlation between ozone and CO_2, and for air in the stratosphere is virtually identical to panel (e) of Figure 2.

Taken together, Figures 2 and 3 suggest that one can think of the middle world observations as characterized by a mixture of stratospheric and tropospheric air, with the stratospheric component during STRAT and POLARIS having different age distributions. The age distribution of lower midlatitude stratospheric air has been thoroughly analyzed by Andrews et al. [2001] using simultaneous in situ measurements of CO_2 and N_2O on the NASA ER2 research aircraft. Strahan et al. [1998] utilized the same in situ CO_2 measurements in the upper tropical troposphere, lower tropical stratosphere and

midlatitude stratosphere to evaluate a CO_2 climatology derived from the Goddard chemistry and transport model. The agreement between the model output and measurements of CO_2 in the lower stratosphere provided evidence that assimilated winds can be used to represent transport in the lower midlatitude stratosphere. Furthermore, this stratospheric age of the air as represented by this climatology allows facilitates parameterizing the latitudinal and altitude dependence of stratospheric tracers used in the mixing model described below.

Based on Figures 2 and 3, in trying to quantify this profile we assume that mixing takes place as subtropical air isentropically follows an anticyclonic flow poleward to northern latitudes and then equatorward. The original middleworld mix of upper tropospheric and lower stratospheric air exiting the subtropics picks up older stratospheric air as its trajectory traverses northern midlatitudes. While details of the causative mixing processes are not available, it is plausible that midlatitude convective activity that occurs in northern midlatitudes in summer (see for example Jost et al., 2004; Pittman et al., 2004), often penetrating the local tropopause, provides the local turbulence that promotes the mixing of stratospheric and convective air masses into the air originating in the UTT. Tracer isopleths that slope downward with increasing latitude relative to isentropic surfaces provide the source of older stratospheric air in these convectively turbulent regions. Additionally, as illustrated in Figure 1, the CF mission occurred by design over an area undergoing significant convection that often penetrates the local tropopause as well. Regardless of how the mixing takes place, or the extent of convective perturbation to the air masses sampled during CF, we want to use simultaneous tracer measurements to determine the fraction of air corresponding to each of the pathways outlined in Figure 1. We choose as a test case the flight of June 29, 2002, the ferry flight from Houston, TX, to Key West, FL.

Mixing Model

Tracers used in the model

Because we are interested in quantitatively differentiating between old and young stratospheric air, tropospheric air from the UTT, and that driven by midlatitude convection, we would hope to use in the model tracers that have signatures might correlate strongly with each of these air mass descriptions. Accordingly, using tracers with different atmospheric lifetimes can be a very powerful tool for analyzing the composition of an air mass. For example, stratospheric and tropospheric water vapor mixing ratios are easily distinguished, while water vapor mixing ratios are relatively invariant to the age of stratospheric air. The ozone mixing ratio is sensitive to stratospheric age, on the other hand. CO_2 not only is sensitive to stratospheric age because of its secular trend, but additional selectivity results from tracking its seasonal cycle in young stratospheric air. Both NO and NOy resulting from lightning can be strong independent indicators of midlatitude or subtropical convective activity, as can (elevated) carbon monoxide and (decreased) ozone. While we will include plots of NO in our figures, we don't use NO data to constrain the model output because of its short photochemical lifetime. The ability of any tracer to distinguish the tracer origins can be most readily illustrated by plotting the source region profiles used in the model.

Source region profiles

To develop source region profiles, we rely where possible on in situ tracer measurements in the UTT and lower stratosphere. We also try to address the complication that in some cases it is difficult to establish that a profile measured in a source region represents only pure air from that region. For example, if we assume that equatorward transport of northern midlatitude air is isentropic, why don't we use tracer profiles measured between 350–390 K for the northern midlatitude source region? The answer is that for the most part, the measured profiles are already mixtures of stratospheric and tropospheric air. To eliminate any ambiguity, we use profiles that are purely stratospheric and then assume that the stratospheric air masses descend as they move poleward, as shown in Figure 5 of Strahan et al. [1999]. We then test the sensitivity of the model to the amount of that descent. Figure 4 shows profiles of the five tracers used in the mixing model.

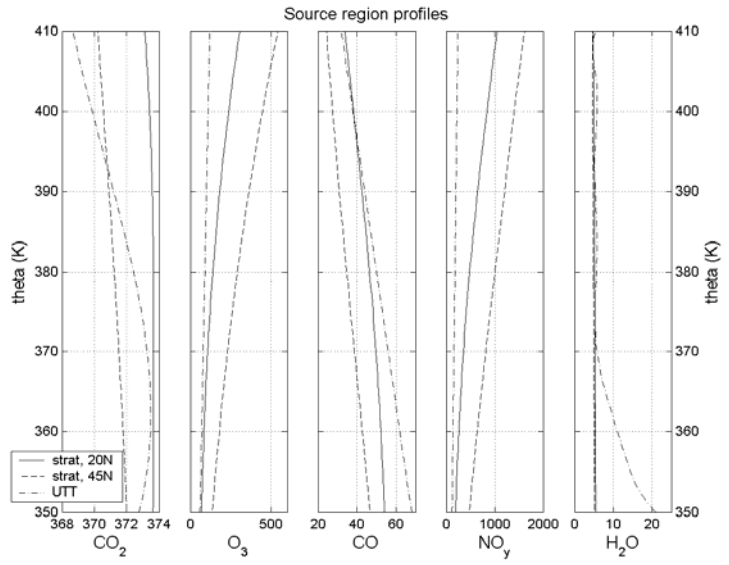

Figure 4. Source region profiles used in the model for young stratospheric air (STRAT 20˚N), older stratospheric air, (STRAT 45˚N), and tropical air (TTL).

For the TTL, all except CO_2 profiles are derived from averaged measurements in the TTL taken on the NASA ER2 aircraft. For NOy, complications can potentially arise from convective influence. While there are fewer lightning flashes in tropical than in midlatitude convection, we nevertheless have removed profiles from the average that are clearly influenced by convection. Carbon dioxide is derived from an average of the Mauna Loa and Samoa ground station data per Boering et al. [1994]. We assume immediate rapid ascent of the air mass from ground level to the 350 K isentrope, followed by an ascent rate of 0.5 K/day through the TTL. The most difficult profile to represent in the TTL is that of water vapor. Air parcels that are isentropically transported into the lowermost stratosphere must cross the extratropical tropopause, and in the process are assumed to be dehydrated potentially to the ice saturation mixing ratio (wvsmr) of the minimum temperature experienced by the air parcel. However, recent relative humidity data illustrate that depending on the density of cloud condensation nuclei, their chemical composition, and local dynamics, dehydration might only reduce the local water vapor mixing ratio to 1.3–1.6 times the wvsmr. [Smith et al., 2003; Jensen et al., 2003]. Additionally, for the air sampled over Key West, the influence of TTL air occurred more than 10 days prior and therefore could not be expected to provide valid constraints on water mixing ratios. Accordingly, the back-trajectory approach would have limited value in our case. Nevertheless, as a check on our assumed TTL water vapor profile we have compared ice saturation mixing ratio profiles from radiosonde data taken in two locations respectively bounded by 15 and 25°N latitude and 75 and 90°W longitude. However, as seen in panel 5, water vapor cannot be used to help distinguish between young and old stratospheric air once there is any tropospheric input.

Stratospheric source profiles that properly represent ozone's latitude dependence are derived from average ozonesonde profiles from Hilo, HI; Wallops Island, VA; Boulder, CO; Goose Bay, Newfoundland; and Churchill, Manitoba. The values of the other tracers as a function of latitude are derived from aircraft-borne in situ profiles taken during the STRAT and POLARIS campaigns and parameterized as a function of ozone. The CO_2 data is adjusted based on its secular trend, as measured at the tropical ground stations (NOAA Carbon Cycle Greenhouse Gases Group). We see that for the tracers plotted in panels 1 to 4, that old stratospheric air is most easily distinguishable from TTL and young stratospheric air, whereas the separation of TTL and young stratospheric is smaller. Only the CO_2 relationship between young stratospheric air and TTL air is complicated by the CO_2 seasonal cycle. It is worth stating again that while the midlatitude stratospheric profiles extend down into the middleworld, there is a parameter in the model that allows for midlatitude stratospheric air to descend from the

overworld into the middleworld, allowing for the mixing in of older air as stratospheric air travels poleward.

A further complication arises when considering young stratospheric air. We could have used modeled profiles with pure tropical character, which do not include older stratospheric air that has been isentropically mixed into the lower tropical and subtropical stratosphere. We chose not to do that because we are distinguishing this from pure tropical air. This means, however, that the TTL and its purely tropical source profiles extend to 410 K, as schematically represented in Figure 1, and are different from the young stratospheric source profiles from 20°N that contain some older stratospheric air mixed in.

Convective sources

The middleworld data during CF were often impacted by convection, as noted by Jost et al. [2004]. Evidence for this was often provided by high lightning-induced NO and NOy, as well as high CO_2 and water vapor. Because of the potential for extremely high convective source terms, small fractions of convected air can cause significant perturbations on the tracer measurements. Pfister et al. [2001] have developed an approach that uses back trajectory calculations combined with GOES infrared imagery, to identify when the air sampled during CF was influenced by convection. We show in Figure 5a isentropic back trajectories calculated using National Center for Environmental Prediction (NCEP) meteorological data originating from points along the 20020629 flight path. The asterisks indicate where trajectories intersect convection, with color-coding indicating the days between convection and the flight date. The squares, color-coded to represent trajectory temperature, indicate the points on the flight track influenced by convection. Figure 5b plots potential temperature and water vapor mixing ratio as a function of time for the flight, along with the points whose back trajectories intersected convection, with the ordinate indicating the days since convection.

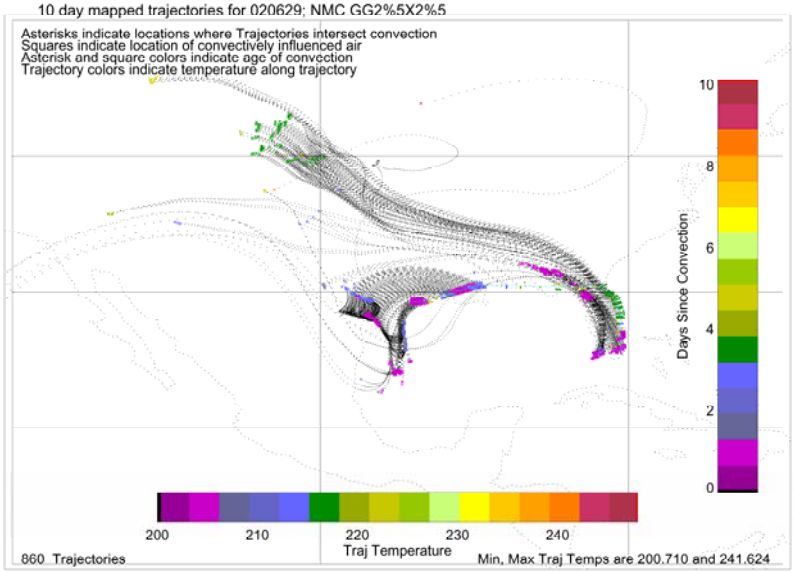

Figure 5a. Isentropic back trajectories calculated using National Center for Environmental Prediction (NCEP) meteorological data originating from points along the 20020629 flight path. The asterisks indicate where trajectories intersect convection, with color-coding indicating the days between convection and the flight date. The squares, color-coded to represent trajectory temperature, indicate the points on the flight track influenced by convection.

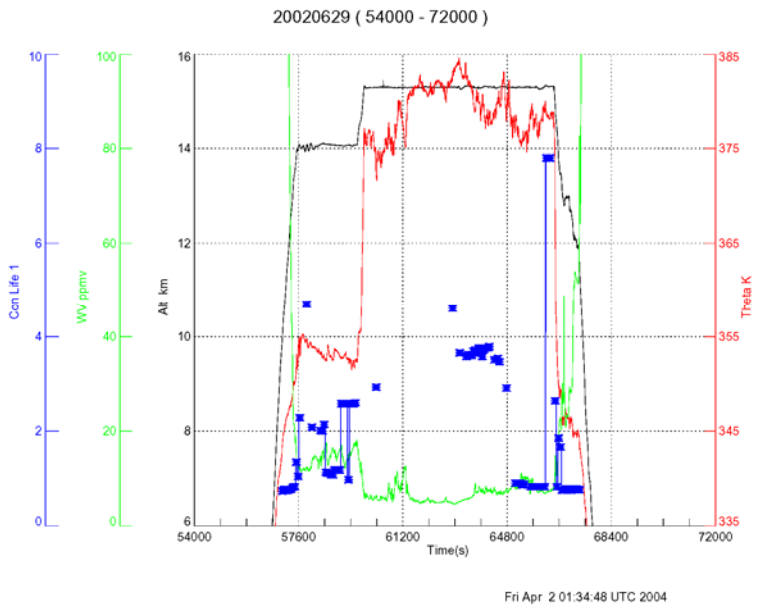

Figure 5b. Plots of potential temperature and water vapor mixing ratio as a function of time for the flight, along with the points whose back trajectories intersected convection, with the ordinate indicating the days since convection.

Using the time, latitude, and longitude of the convective event and a Receptor-Oriented Atmospheric Modeling (ROAM) framework [Gerbig et al., 2003], CO and CO_2 mixing ratios convectively transported into the upper troposphere are derived from their respective boundary layer observations. ROAM incorporates (1) a backward-time Lagrangian particle transport model called the Stochastic Time-Inverted Lagrangian Transport (STILT) Model [Lin et al., 2003] driven with analyzed meteorological fields and parameterized turbulence. The lightning induced NOy values are calculated based on lightning strike data from the National Lightning Detection Network [Pickering et al., 1998]. Ozone boundary layer values used to represent convective source values are based on ground ozone monitoring stations in geographic regions where convection intersected the back trajectories. For the convective sources in the Colorado and Kansas areas, we use 35 ppbv, which is an average of eight ground station reports in Colorado for the period of June 18–28. For the convective sources in eastern Texas, an average of nine ground stations in eastern and central Texas for the period of June 26–28 gives a value of 34 ppbv ozone. Daily measured values averaged over 17 Florida monitoring sites for June 26–29 was invariant at about 28 ppbv, with no averaged daily values at any site being more than 40 ppbv. Nevertheless, for this analysis, we test the model by varying the convective input to test model sensitivity to plausible inputs, since our first goal constrain its impact on the uncertainty of our results. However, quantifying the convective component is important for a number of reasons. It is clear that convection, both in the tropics and in midlatitudes, has the potential for transporting boundary layer pollutants into the TTL and lower stratosphere. Trends or increases in the frequency and intensity of convective events brought about by global change could accordingly have a significant impact on trace species mixing ratios in therein. Using a ROAM framework that provides boundary layer CO_2 values and a cloud-resolving model that uses that uses that data to determine the distribution of CO_2 in cirrus clouds, Xueref et al. [2004] have performed a case study that exhibited quantitative agreement between calculated and measured differences between clear air and cirrus cloud CO_2 mixing ratios in the upper troposphere. It remains to be determined how best to use measurements to quantify on a broader basis the impact of convection on the stratosphere as a whole, and whether there are aspects of global change conspiring to increase this impact. Accordingly, quantify for all of CF the altitude dependence of fraction of convective air sampled during CF, its variability, and possible cause of this variability, would be very useful.

Model details

The model uses a constrained least squares fitting algorithm to minimize the equation $C \bullet x - P = 0$, where C is a matrix whose columns are the tracer mixing ratios in air from the different source regions

corresponding to the potential temperature for each measurement; x is a vector containing the fractions of air from each component; and P is a vector containing the mixing ratio of the tracers as measured by the WB57. In this way, the equation is solved independently for each time at which all the tracers are measured. Each tracer in the fitting algorithm is weighted according to its uncertainty relative to its observed range of values in the applicable potential temperature region. The source regions used in the analysis correspond to the four illustrated in Figure 1, where the specific latitudes of the air corresponding to "young" and "old" stratospheric air used in the model runs presented in the manuscript are 20°N and 45°N respectively. Additionally, because we are assuming that the stratospheric components have descended into the lowermost stratosphere from the lower stratosphere, we can vary this descent in potential temperature units for each latitude, but maintain the same descent value for all data points in each flight or model run.

Results and Discussion

As a test case, we have chosen the 20020629 ferry flight from Houston to Key West because of the tracer variability observed within narrow potential energy bands. We first plot the flight trajectory on the 29th. The airplane remains at about 354 K for the first 35 minutes after climbout from Houston, then ascends to about 380 K for the remainder of the flight, before landing in Key West.

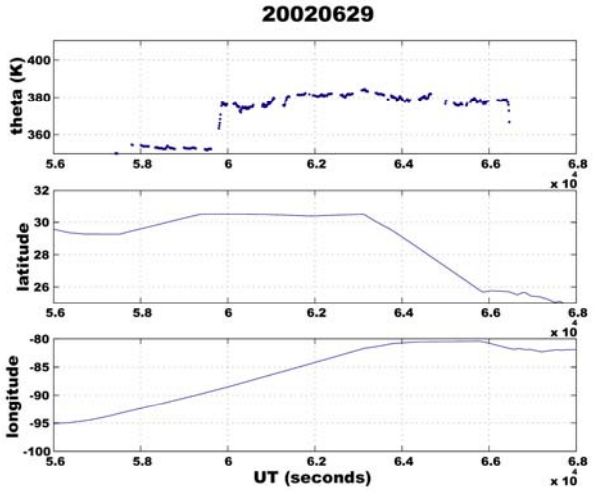

Figure 5. Plots of potential temperature, latitude, and longitude for the 20020629 flight.

An added complication to the analysis during the first segment of the flight is the prevalence of cirrus clouds. In Table 1 we show the various tracer source region combinations used in the respective fits to the measured data. In order to explore the degree to which the model results depend on the combination of tracers used, we begin by using the four tracers: ozone, carbon dioxide, NOy, and carbon monoxide. We leave out water vapor in the first run for two reasons. Firstly, there is a larger uncertainty in its TTL source profile because of the variability in TTL water vapor brought about by convection. In principle back trajectory calculations and/or temperature measurements in the TTL could constrain the relative humidity of the air mass based on assumptions about dehydration of the air parcel. However, the sample air parcels were typically not in the tropics within ten days prior to their being sampled so there is no reliable way to estimate the minimum temperature on which to base dehydration. Secondly, by first leaving out water in the model we illustrate how critical it is for these analyses. We include two runs using the same convective inputs but with different end members for the older stratospheric component to illustrate the level of uncertainty by what could be considered a fairly subtle change in the end member values for this transport pathway.

Table 1. Summary of conditions used in each mixing model run. The first two columns show the tracers used for each model run, with fractions of TTL, young stratospheric, and older stratospheric air being mixed to match the measured tracer values. For each of the last two runs, a convective input is added, using the values for each tracer in the respective cell. For the third model run we use old stratospheric air from 40°N that has descended by 30 K and for the fourth run we use air from 50°N that has descended by 20 K.

Tracer	1 Tracers used; no convection	2 Tracers used; no convection	Convective input for 3 & 4
CO_2	X	X	374.5 ppmv
O_3	X	X	30 ppbv
CO	X	X	250 ppbv
NOy	X	X	3000 pptv
H_2O		X	50 ppmv

In Figure 6 we plot the calculated percentage of air from each source region for each of the four model runs for the 20020629 flight. For each of the five tracers we plot versus time the measured and calculated tracer mixing ratios, where the calculated mixing ratio, $(tracer)_{calc} = \Sigma_i\ fr_i * tracer_i$, where the sum is taken over each of the source regions and $tracer_i$ represents the end-member value in the corresponding source region for each tracer and fr_i represents the calculated fraction of air from that source region. Included as well is the average fraction from each source region, plotted as a solid line, used just as a visual aid to help provide a sense of the spread in the data. In Figure 7 we illustrate the results of the model for all the data points in the middleworld and lower stratosphere. There are four regions during this flight that we wish to explore: the first is the period after ascent where the aircraft stays near 350 K; the second is the first half of the 380 K portion of the flight; the third is a small segment of this region starting at about 60,800 seconds, lasting about 600 seconds, but with a data gap in the middle caused by a CO_2 instrument calibration cycle; the fourth is the last half of the 380K segment that starts when the aircraft turns southward from 30°N at about 63,000 seconds.

We start by comparing the fit with four tracers, leaving out water vapor, and the fit including water vapor, just to explore how well model fits can be obtained for an incomplete set of tracers. The major change between the fits with and without water vapor included is evident in the early part of the flight, near 350 K, during which time calculated water is at best 50% below measured water vapor. Similarly, CO is about 60 to 75% of its measured value during this part of the flight. When water is included in the model, the improvement for water vapor and CO is significant, albeit better for water. Nevertheless, good agreement results only when a convective contribution is included. For the 350 K region, the fits are virtually indistinguishable for the two model runs that include convection because there is virtually no contribution from older stratospheric air. To summarize, the model shows that about 70% of the air here is young stratospheric air, about 15% TTL air, 7.5% older stratospheric air, and 5% convective air. In the second region, after the aircraft climbs to about 380 K at 30°N, the air becomes about 70% older stratospheric air, 7% young stratospheric air, 15% tropical air, and is less than 1% convective air. However, in the middle of this section of the flight, air is traversed that exhibits unusually high water vapor, elevated CO_2, and reduced ozone. For these data, the model gives a convective input of about 1–4%. While this does not seem like much, it increases the water vapor mixing ratio by more than 5 ppmv, or a factor of 2. While there is a very large uncertainty in both the fraction of convective air present in this region, and a corresponding uncertainty in the end member mixing ratios in the convective air mass, there is significantly less uncertainty in the contribution convective air is making to the water vapor mixing ratio.

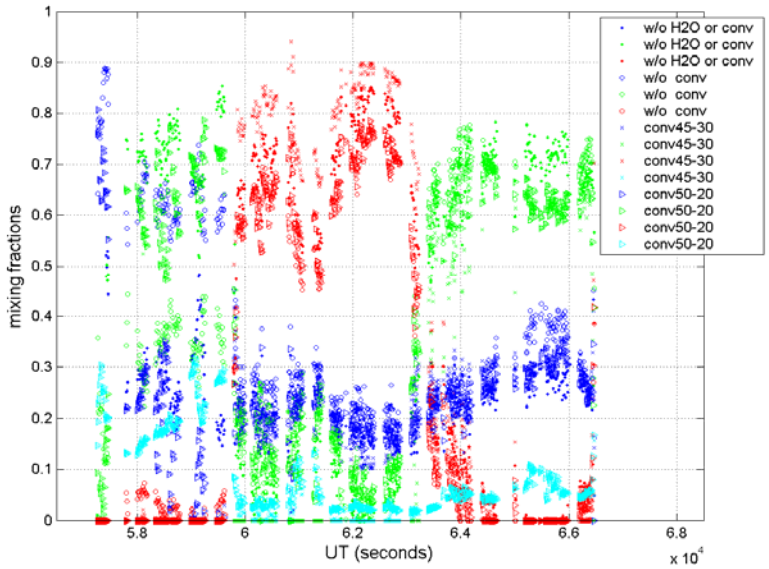

Figure 6. Plots of the fraction of air from each of the four source regions for four different model runs as described in the text, color-coded according to source region, with the different symbols denoting the different model runs. The solid lines represent the average of the four runs and is just used to help see the spread in the model output.

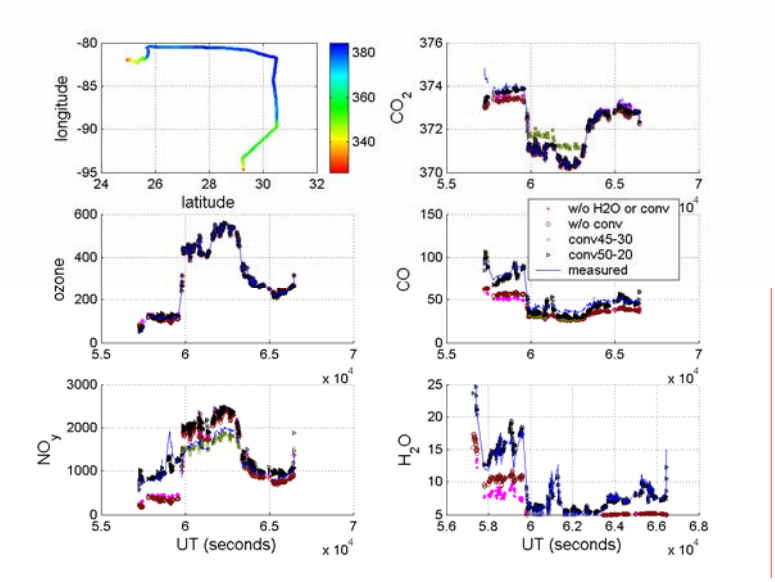

Figure 7. The top left panel again shows the flight profile. The other panels compare the calculated tracer mixing ratios for the four model runs compared to the measured mixing ratios, with the legend valid for all the profiles. The legend delineates for all the tracers the model output for each of the four runs.

Tracer-tracer correlations during 20020629

An ultimate question is whether you can use tracer-tracer correlations to either test the consistency of the model or to use them to estimate or constrain chosen end-member mixing ratios. For example, if one were to try to analyze middleworld mixing in air masses sampled during the STRAT campaign, the work of Hintsa et al. [1998] could provide end-member mixing ratios for the TTL air that has mixed isentropically into the lowermost stratosphere. Similarly, the recent analysis of convective influence during CF by Ray et al. [2004] could serve as another example. Ray analyzed the contribution to the airmass observed over Florida on July 7 and 9 from a convective event that entrained the effluent of a forest fire over eastern Canada. The residuals of the convective plume remained clearly visible near 380 K when the air was sampled over Florida. Analysis that included allowance for ozone production in the plume as it traveled equatorward allowed determination of the convective end-member mixing ratios and

then the fraction of convective air in the sample. It is of interest to determine whether this technique has general applicability. During the June 29 ferry flight there are two particular regions where we can explore whether tracer-tracer correlations can be used to complement the model analysis. The first is in the early part of the flight, during which the aircraft cruises at about 14.7 km, equivalent to about 355 K. Analysis in this region is complicated by the presence of thin cirrus, suggesting that the air sampled around 355 K is influenced by local convection. The second region is comprised of a short segment of the flight when the aircraft is cruising at about 15.8 km, between 60,700 and 61,900 seconds UT and most easily characterized by the more than 5 ppmv increase in water vapor.

In Figures 8 and 9 we illustrate the relevant tracer-tracer correlations, color-coded as described in the figure legends. The times between 60,000 and 66,000 seconds correspond to the 15.8 km cruise, and the segment between 60,700 and 61900 seconds corresponds to the convectively influenced region at 15.8 km. If we start by looking at the O_3:H_2O correlation in Figure 8, we see the parts of a typical correlation plot where the high water low ozone region in the top left quadrant corresponds to tropospheric air and the high ozone low water vapor region is in the bottom right quadrant is representative of stratospheric air. Points made up of a mixture of air from these two regions with low ozone and low water vapor mixing ratios are in the bottom left quadrant. However, this plot shows deviations from this simple tracer-tracer correlation in the form of air containing relatively constant ozone with a range of water mixing ratios. In this case there are two of these, one with ozone about 410 ppbv, occurring at 15.8 km and the other with about 115 ppbv ozone and occurring at about 14.4 km. A quick look at the other plots show that, like ozone, CO_2 and CO (not shown) behave similarly to ozone. The evaporation of cirrus cloud ice particles is the most likely explanation of this. On the other hand, NOy does show variability. The H_2O-NOy correlation shows that for the lower altitude convectively influenced region, the high water air masses are characterized by three to four different NOy values. However, further inspection shows that most of the NOy variability occurs within cloudy regions, and the rest is most likely a result of recent particle evaporation, as shown in Figure 9 where the data are binned by particle density. In the high altitude convectively influenced region NOy behaves like ozone and the other tracers, with no evidence of NOy released as particles evaporate. So, the convective influence in the air sampled during this flight cannot be quantified using the approach Ray used. However, the tracer-tracer correlations do illustrate that it is very difficult to devise an approach that constrains both the end-member values of the convective air masses and the corresponding fraction of convective air. Instead, we constrain the total amount of each tracer contributed by convection. It is important to realize that an air mass sampled in the lowermost stratosphere has often been perturbed by more than one convective event and our analysis only derives the total convective perturbation.

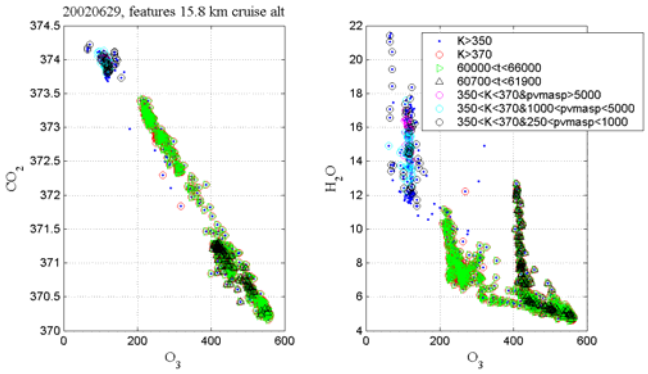

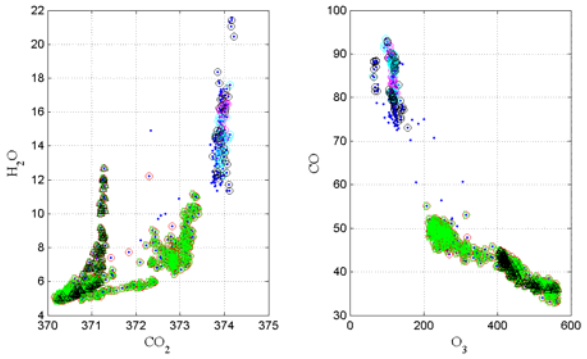

Figure 8. Tracer-tracer correlations for 20020629 flight. Data in all the panels are color-coded according to the legend. The last three designations in the legend distinguish between data points taken when cirrus particle volumes were greater than 5000 μ^3/m^3, between 1000 and 5000 μ^3/m^3, and less than 1000 μ^3/m^3.

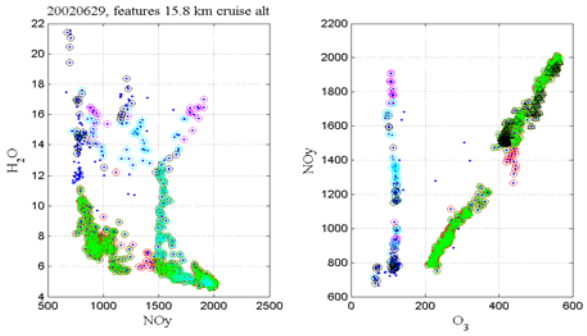

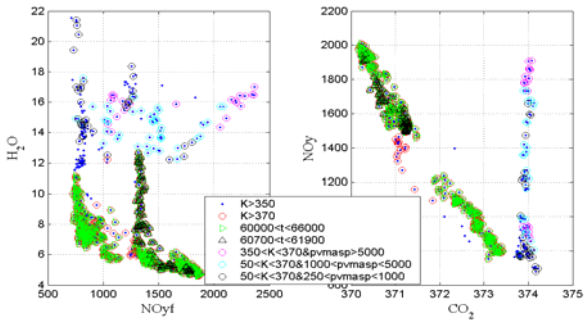

Figure 9. Tracer-tracer correlations for 20020629 flight, as in Figure 8.

We see that the air masses influenced by convection can only be slightly differentiated from the other air masses. For any given ozone mixing ratio, the range in CO_2 is typically only 0.25 ppmv and in the convectively influenced air mass, it increases by 0.5 ppmv. On the one hand this might be attributed to the narrow range of CO_2 stratospheric values. However, the amplitude of the CO_2 seasonal cycle in the stratosphere is about 3 ppmv and the range of CO_2 values observed in the boundary layer could easily extend from 365–380 ppmv. This suggests that it is coincidental that the low ozone high CO_2 points fall on the same tracer-tracer correlation line. It is more instructive to look at the convectively perturbed region.

It is the correlations with water that provide the most air mass differentiation capability. Starting with water versus ozone, we see that the points below 370 K, most of which cluster around 355 K, show the influence of two distinct convective air masses, most with about 100 ppbv ozone, with the other having about 70 ppbv ozone. We identify this as convective because of the large range of water vapor mixing ratios in air masses having the same ozone mixing ratios. A look at the water CO_2 correlations shows that for both cases the CO_2 mixing ratio is virtually constant. Now, if we look at the NOy:water correlation plot, we see even further differentiation in the air masses. This correlation is even more pronounced in a total NOy:total water correlation plot, showing that these clouds were not formed in situ but represent convective ouflow cirrus. While in-cloud and clear-air ozone mixing ratios are virtually the same, CO mixing ratios are up to 10 ppbv higher in the cloud while ozone and CO_2 values are virtually indistinguishable. We can use these correlations plots to constrain the convective end member values for the model as follows:

1. CO_2(convective) = 374 ppmv
2. O_3(convective) = 115 ppbv
3. CO(convective) = 100 pptv

It is difficult to constrain NOy. In cloud-free air, NOy is about 800 ppbv, and increases from there with particle volume as measured by the multiangular scattering probe (MASP). We can roughly scale the convective sources of NOy and water vapor in the ratio of 1 ppmv (H_2O) to 100 pptv NOy based on their maximum values in the region. Accordingly, we could try convective end-member values with that ratio in the model. The difficulty with this approach is that it is limited to constraining the impact of the local convection on the air mass, but not the cumulative impact. It is clear that region that shows evidence of evaporating cirrus clouds that contain NOy in excess of the local NOy concentrations, are adding to the impact of previous convective events. Accordingly, we do not pursue this approach.

It is interesting to now turn to the high water event at 15.8 km. Here, water increases to 13 ppmv while neither ozone, CO_2, CO, nor NOy are perturbed from ambient mixing ratios in any significant way. The only explanation for this observation is the evaporation of overshooting ice particles, followed by mixing lines between the air with enhanced humidity and the surrounding air. This type of feature is not representative of one that typifies a convective air mass that might contain not only enhanced water vapor, but also tracer mixing values representative of boundary layer and tropospheric air entrained in the convective plume.

Having tested the model on the ferry flight, and given the constraints on the model's capability, the questions the model can most directly address are:

1. During the CF campaign, how much did the equatorward flow caused by the monsoon impact the lowermost stratosphere over Florida?
2. How much did convection impact the lowermost stratosphere during the same period?
3. What impact might the combination of midlatitude convection and equatorward flow have on air eventually becoming part of the general circulation?

To address these questions we refer to Pittman et al. [2004], which uses back trajectory calculations and tracer-tracer correlations to illustrate the changes that took place during July in the pathways transporting air into the lowermost stratosphere over Florida. Based on their analysis, the authors separate the flight data into three regimes during the beginning, middle, and end of the month, for which back trajectories indicated distinctly different transport pathways. To investigate the impact of the

three trajectory patterns, we bin the tracer data in 1-degree units of potential temperature for each of the three regimes. We then determine for each regime the best fit, as for the example of 20020629. Table 2 shows the convective end members used for fitting the data in the three regimes. We note once again that the model does not constrain the convective end member, but rather the product of that end member and the fraction of convective air.

Table 2.

Tracer	Convective input, Regime 1	Convective input, Regime 2	Convective input, Regime 3
CO_2 (ppmv)	374.5	374.5	374.5
O_3 (ppbv)	30	30	30
CO (ppbv)	500	350	300
NOy (pptv)	3000	12000	6000
H_2O (ppmv)	200	125	200

Using these end members and assuming the older and younger stratospheric air end member values from 20°N and 45°N that has descended by 30 K, we show in Figures 10–12 the model results for the three regimes. In each figure we plot the average value of the tracer binned in 1 K units, the comparable calculated tracer mixing ratios, and, except for CO_2, the contribution from each source region. In the bottom right panel, we plot the fraction of convective air for the three tracers for which convection can be the dominant source. For CO_2, the fractional contribution form each source region is of little interest, so we only show the agreement between measured and modeled CO_2.

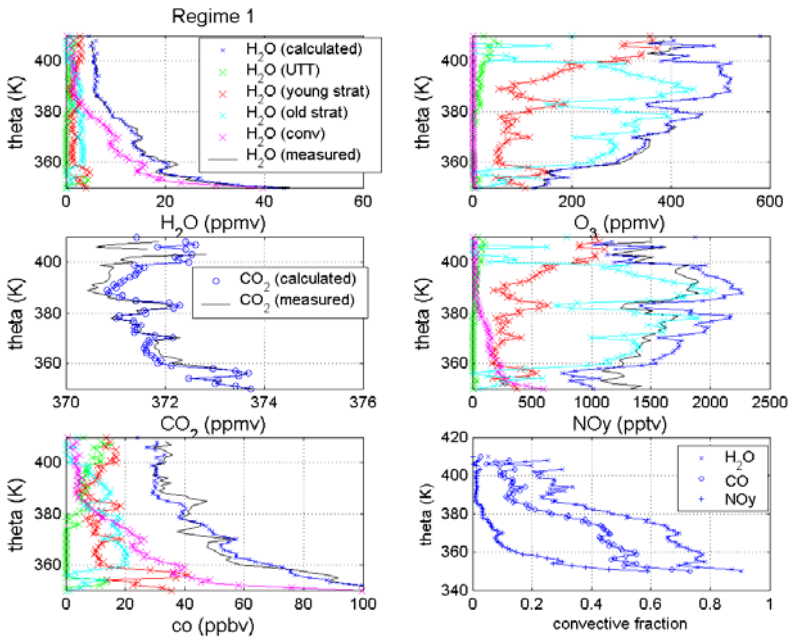

Figure 10. we plot the average value of the tracer binned in 1 K units, the comparable calculated tracer mixing ratios, and, except for CO_2, the contribution from each source region. In the bottom right panel, we plot the fraction of convective air for the three tracers for which convection can be the dominant source. For CO_2, the fractional contribution form each source region is of little interest, so we only show the agreement between measured and modeled CO_2. The legend in the top left panel is valid for the plots of the other tracers as well.

Starting with water vapor, the most startling result from the model is that even around 380–390 K, the convective contribution to water vapor is significant. The water vapor mixing ratio starts increasing sharply at about 388 K, and this increase might normally be thought to be a result of air from the tropics not being dehydrated to the expected 6 to 7 ppmv. In fact, if this were the case, and the air was purely tropical in character, ozone would be much lower, certainly less than 200 ppbv. The model shows that only convective influence along with older stratospheric air can allow for fitting all the tracers used. Because the TTL end member profile extends up to 410 K, the model actually allows for TTL air to be mixed in up to 410 K as well. Results in this region might be intriguing but are certainly more uncertain than those below 390 K. The model also shows very significant convective contribution to NOy and CO

as well. The CO contribution and its implications have already been thoroughly discussed by Jost et al., [2004]. The NOy contribution is of interest because the NO from lightning is the source of this NOy and during its approximately week-long lifetime in the stratosphere, it contributed to ozone loss through the NOx catalytic cycle.

It is clear that convection does not significantly influence ozone because typically convected air contains much less ozone than stratospheric air and somewhat less that TTL air. Because there is intense interest in the control of midlatitude ozone in the lowermost stratosphere we need to carefully explore the implications of the model on ozone. The model shows that in regime 1 older stratospheric air, not unexpectedly, provides most of the ozone, with young stratospheric air the source of the remainder. There is one feature just above 380 K with an increase in young air, as shown most simply by decreasing ozone and NOy, and increasing CO_2. It is clear that ozone variability can be very large in the lowermost stratosphere and ozone can be dominated by the amount of fraction of older stratospheric air. Accordingly and not unexpectedly, the strength of the summer monsoon will strongly impact measured ozone in the midlatitude lowermost stratosphere.

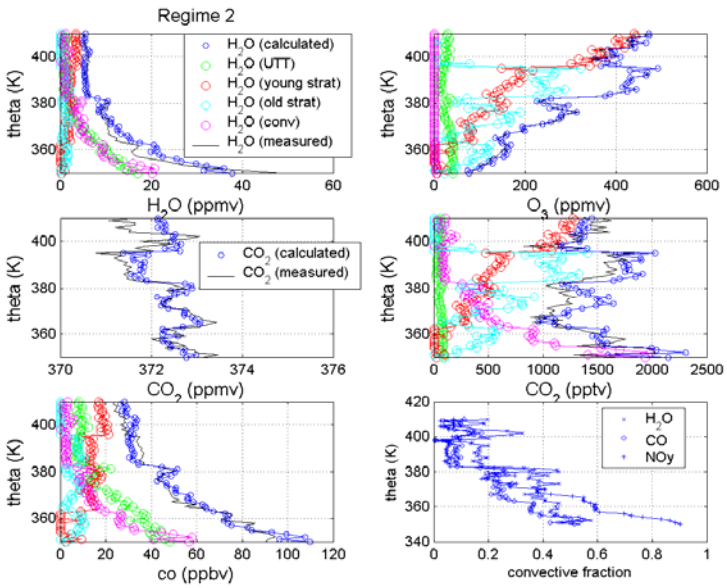

Figure 11. As in Figure 10, but for regime 2.

Comparing the results in regimes 2 and 3 with regime 1, we note that during regime 2 there is a lower fraction of older stratospheric air than in regime 1; similarly, the convective contribution above 370 K has decreased as well. Below 370 K, convection dominates as the NOy source, while for CO and water vapor, the TTL and convective sources provide about the same contribution. In regime 3, the contribution of older stratospheric air has decreased even further near 380 K, but the feature still remains between 360–370 K. The model shows that near 380 K, CO and water vapor are dominated by TTL air, then decrease as TTL air is replaced by older stratospheric air below 370 K, and then increase as both the TTL and convective contributions increase with decreasing potential temperature.

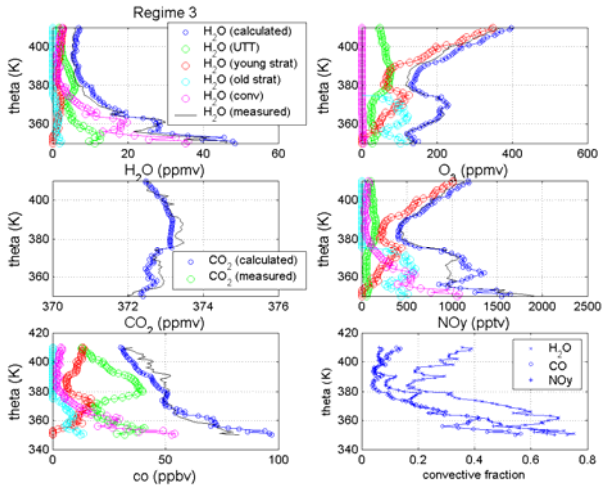

Figure 12. As in Figure 10 but for regime 3.

Figure 13 shows the fraction of air from each source region for each regime. This plot most clearly shows the transition in regime three to a large TTL component between 380–390 K, as well as the largest contribution of old stratospheric air during regime 1. It is interesting to note that during regime 1 there is virtually no attribution to TTL air and, except for a unique contribution during regime 1 between 350–360 K, the contribution of young stratospheric air declines with theta, as expected. The model increases the contribution of young stratospheric air in this region, rather than TTL air, because of the relatively high CO coupled with the increase in CO_2. The seasonal cycle of CO_2 helps constrain the model to use young stratospheric air rather than TTL air. Additionally, if we refer back to Figure 6, we note that the model identifies 50–60% of the air around 355 K as young stratospheric air. Nevertheless, we investigate how robust this feature is to both to the age of the young stratospheric air and the chosen convective inputs. All the stratospheric tracer profiles were derived from summertime STRAT and POLARIS data. This does not allow for the possibility, or even likelihood, that the average time it takes air between 380–420 K between 30 and 45°N to descend to 350–380 K between 45 and 60°N is on the order of a few months. This transit time can be assessed by carefully comparing CO_2 and water vapor mixing ratios in the two regions of interest because their respective seasonal cycles can help resolve the different transit times [Boering et al., 1995]. Analysis of the limited lowermost stratospheric data available from POLARIS show that the young component of the air entered the stratosphere in the spring. This represents a transit time from the topical tropopause region consistent with that shown by the lowermost stratospheric air sampled during POLARIS at high latitudes. While this validates the reference profiles used for midlatitude stratospheric air, it is still useful to test the model sensitivity to the CO_2 and H_2O profiles that will exhibit a seasonal dependence not evident in the other tracers. Substituting ozone:CO_2 and ozone:H_2O correlations derived from spring midlatitude stratosphere POLARIS data results in negligible differences to the model fits.

It is interesting that the convective contribution during all three regimes appears to be virtually identical, contributing about 0.7% of the air just above 380 K, and gradually increasing with decreasing theta to about 8% near 360 K and 18% at 350 K. However, it is not the fraction of air but the actual tracer contribution that is important. In the left panel of Figure 13 we see how the convective contribution to water vapor, carbon monoxide, and NOy, vary with potential temperature or the three regimes. The interesting question is how do the convective inputs differ in the three regimes. For example, between 360 and 380 K, regime 1 is mostly older stratospheric air. The convective contribution to water vapor is highest during this regime from a fractional perspective, averaging about 65%, somewhat lower during regime 2, averaging about 40%, and extremely altitude dependent in regime three. However, from an absolute standpoint, regime 2 is somewhat lower than regimes 1 and 3. This contrasts with NOy, for

which the highest contribution is during regime 2. The convective contribution to CO, like water vapor, is highest in regime 1.

While the figures show that there are differences in the convective contributions in the three regimes, can we correlate these differences with the fraction of old stratospheric air? For example, the air mass in regime one between 360–380 K is mostly old stratospheric air, and water vapor and CO show a commensurate increase in convective influence, whereas NOy does not. The convective contribution of water vapor and CO also show a dip below 360 K, in agreement with the transition to the decrease in older stratospheric air. In regime 2, the increase in old stratospheric air occurs sharply at 390 K, yet the increase in convective influence occurs sharply at 380 K, thus imposing an upperbound on the convection that contributed to the sampled air masses.

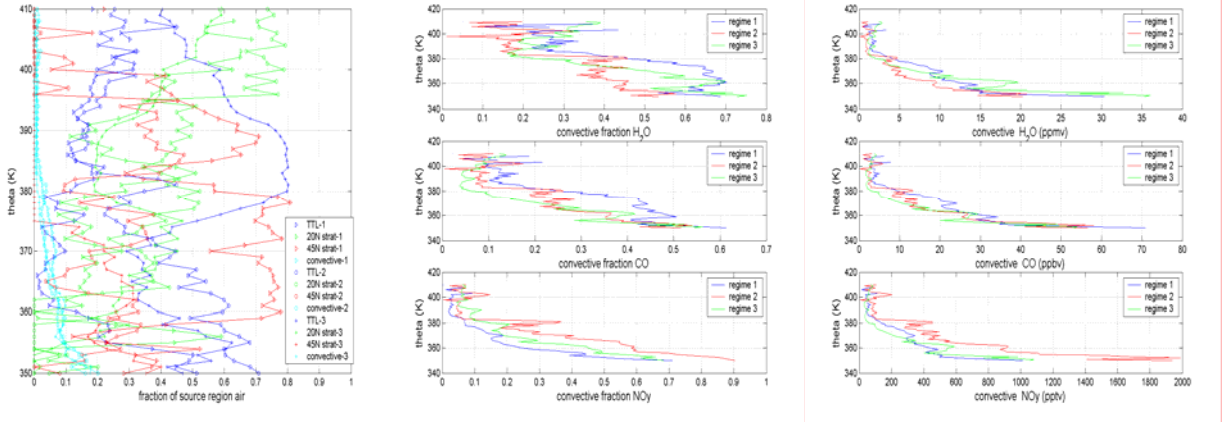

Figure 13. On the left, the fraction of air from each source region is plotted for each regime. The legend identifies contribution from each of the source regions for the three regimes separated by time during the month of July. In the middle and on the right, the convective contribution to the listed tracers is plotted for each regime in fractional and absolute terms.

We next evaluate the sensitivity of these results to the model uncertainties that are most difficult to quantify. Figure 14 focuses the first regime to illustrate the dependence on convective input. We use three different convective inputs as detailed in the figure caption, which give comparable fits to the tracer profiles. We do this to especially test the sensitivity below 370 K where the convective input has the greatest impact. The figure shows how between 360–380 K the different convective end-members have a measurable impact. Below 360 K the plot illustrates that slight changes in the convective end members can create large changes in the calculated fractions of TTL and stratospheric air. However, if we evaluate the quality of the fit by summing the square of the residuals for all the points in the model run, $\Sigma[(tracer_m - tracer_c)/tracer_m]^2$, we get for the three model runs 0.0825, 0.0636, and 0.0547. This suggests that the feature near 355 K that shows a dominant contribution from young stratospheric air is robust. This, as expected, is consistent with the analysis of 20020629 data in the same region. Note also that the convective contribution is reasonably independent of the convective end-members input into the model., This does not appear to be the case for NOy, in part because the degree to which modeled NOy is overestimated is worse in the first two runs.

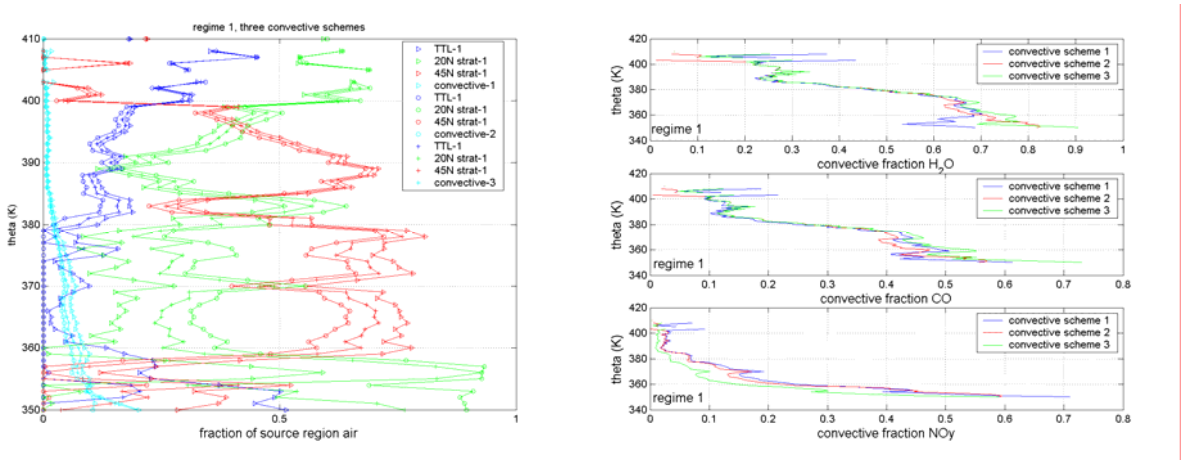

Figure 14. Fraction of air from each source region plotted for regime 1, with the only change being the convective input values. Case 3 convective values are identical to those in Table 1. Case 2 decreases CO_2 from 374.5–365 ppmv and doubles NOy from 3000–6000 pptv. Case 1 increase CO_2 to 380 ppmv, decreases CO from 500–350 ppbv, decreases NOy to 5000 pptv, and decreases H_2O from 200–150 ppmv. The right-hand panel shows the sensitivity of the convective contribution of the plotted tracers on the convective end-members used in the model run.

In the left panel of Figure 15 we focus on the sensitivity to the age of the stratospheric air that has descended into the middleworld. For the three runs with the stratospheric descent as described in the legend the respective residuals are virtually the same at 0.0825, 0.0804, and 0.0880. This suggests that we can not objectively choose between the three options, for the region near 380 K. However, the last run attributing the air in this region to be 90–95% old stratospheric would seem to be the outlier, and it does provide the worst fit. In all cases the tracer that has the largest residuals is NOy, and that is in part caused by the proscribed weighting factors in the least squares fit. Both NOy and CO are given 10% uncertainties in the model, compared to 5% for water vapor, 1% for ozone, and 0.1 ppmv for CO_2. The apparent systematic offset between measured and modeled NOy, especially in the stratosphere, is consistent with the ratio of the NOy-ozone correlations measured in the stratosphere during CF and that derived from STRAT and POLARIS data. Increasing measured NOy by 25% to account for that difference has a negligible effect on the results. In the right panel of Figure 15 we plot the convective fraction of water vapor, carbon monoxide, and NOy. The three descent scenarios do not significantly impact the convective input. The combination of figures 14 and 15 illustrate that even without being able to constrain the end-member convective values, the convective contribution to the lowermost stratosphere is constrained by the model.

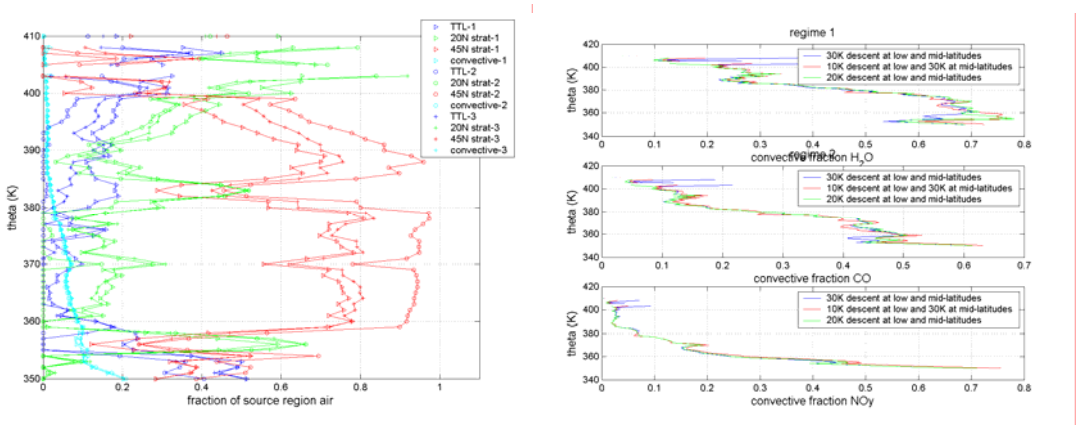

Figure 15. In the left panel we plot fraction of air from each source region as designated in the legend for the three stratospheric air descent scenarios shown in the legend on the right. The right-hand panel shows the sensitivity of the convective contribution of the plotted tracers on the stratospheric descent parameter used in the model run.

Conclusions

Understanding how the composition of air in the lowermost stratosphere is controlled is vital for understanding issues including midlatitude ozone depletion, the relative humidity in the region and thus the formation and evolution of thin cirrus near the tropopause, the potential for equatorward transport of air that can ascend radiatively and enter the general circulation. Processes that are preferentially active during the summer, such as convective activity, coupled to monsoonal circulation patterns, serve to both complicate the analysis of the region and make its understanding more critical. The CF campaign provided a unique opportunity to study the region. Using simultaneously measured tracers, a simple box model illustrates that air from all four source regions described in Figure 1 can provide important contributions to the air in the lowermost stratosphere between 360 and 390 K. The variability in the age and fraction of the stratospheric component is the prime reason for ozone variability observed in the region. While small contributions from the troposphere can obviously reduce ozone, small contributions of older stratospheric air can similarly increase it. These results provide important implications for potential impact of global change both on midlatitude ozone through the convectively-induced increase in water vapor and NOx in the lowermost stratosphere, through the relative strengths of transport pathways into the region, and through increases in stratospheric water vapor from a combination of midlatitude convection and equatorward flow.

One of the most interesting features of the model is that the water vapor contribution is significant even up to 380 K, and the feature is very robust. While the NOy contribution is less robust, in part because there are large uncertainties in the convective end-members and significant uncertainties in the stratospheric end-members, the analysis does shoe that convection is a significant source of NOx up to 380 K as well.

The utility of this kind of analysis goes beyond the analysis of mixing in the middleworld of long-lived tracers without considering chemical reactions along back trajectories. Ultimately, we have developed a framework that can be used to start with end-member values that mix with ambient air in a parameterized fashion as the air parcels follow back trajectories to the time and place they are sampled.

References

Bannister R., A. O'Neill, A. Gregory, and K. Nissen, The role of the S. E. Asian monsoon and other seasonal features in creating the tape-recorder signal in the Unified Model, Abstract O-5-03, third SPARC General Assembly, August, 2004, Victoria, British Columbia, CA.

Chen, P, Isentropic cross-tropopause mass exchange in the extratropics, *J. Geophys. Res.* **100**, 16,661–73, 1995.

Dunkerton, T, Evidence of meridional motion in the summer lower stratosphere adjacent to monsoon regions, *J. Geophys. Res.* **100**, 16,675–88, 1995.

Conway, C. L., et al., CMDL Summary Report #27, Chapter 2, Carbon Cycle greenhouse gases, NOAA CMDL, Boulder, CO, 2003.

Fischer H., D. Brunner, G. W. Harris, P. Hoor, J. Lelieveld, D. S. McKenna, J. Rudolph, H. A. Scheeren, P. Siegmund, H. Wernli, J. Williams, and S. Wong, Synoptic tracer gradients in the upper troposphere over central Canada during the Stratosphere-Troposphere Experiments by Aircraft Measurements 1998 summer campaign, *J. Geophys. Res.* **107** (D8), doi:10.1029/2000JD000312, 2002.

Fueglistaler, S., H. Wernli, T. Peter, Tropical troposphere-to-stratosphere transport inferred from trajectory calculations, *J. Geophys. Res.* **109**, D03108, doi:10.1029/2003JD004069, 2004.

Gerbig, C. et al., Towards constraining regional scale fluxes of CO2 with atmospheric observations over a continent: 2. Analysis of COBRA data using a receptor oriented framework, *J. Geophys. Res.* **108** (D24), 4757, 2003.

Hegglin, M.I., D. Brunner, H. Wernli, C. Schwierz, O. Martius, P. Hoor, H. Fischer, U. Parchatka, N. Spelten, C. Schiller, M. Krebsbach, U. Parchatka, U. Weers, J. Staehelin, and Th. Peter, Tracing troposphere-to-stratosphere transport above a mid-latitude deep convective system, *Atmos. Chem. Phys.* **4**, 741–56, 2004.

Hoor P., H. Fischer, L. Lange, J. Lelieveld, and D. Brunner, Seasonal variations of a mixing layer in the lowermost stratosphere as identified by the CO-O 3 correlation from in situ measurements, *J. Geophys. Res.* **107** (D5), doi:10.1029/2000JD000289, 2002.

Hoor, P., H. Fischer, L. Lange, J. Lelieveld, and D. Brunner, Seasonal variations of a mixing layer in the tropopause region as identified by the CO-O3 correlation from in-situ measurements, *J. Geophys. Res*. **107**(5), 10.1029/2000JD000289, 2002.

Hoor, P., C. Gurk, D. Brunner, M.I. Hegglin, H. Wernli, and H. Fischer, Seasonality and extend of extratropical TST derived from in-situ CO measurements during SPURT, *Atmos. Chem. Phys. Discuss.* 4, 1691–726, 2004.

Hudson, D. R., D. F. Alexander, M. F. Andrade, and M. B. Follette, The total ozone field separated into regimes. Part I: Defining the regimes, *J. Atmos. Sci.* **60**, 1669–77, 2003.

Jost, H.-J., K. Drdla, A. Stohl, L. Pfister, M. Loewenstein, J. P. Lopez, P. K. Hudson, D. M. Murphy, D. J. Cziczo, M. Fromm, T. P. Bui, J. Dean-Day, C. Gerbig, M. J. Mahoney, E. C. Richard, N. Spichtinger, J. V. Pittman, E. M. Weinstock, J. C. Wilson, I. Xueref, In-situ observations of mid-latitude forest fire plumes deep in the stratosphere, *Geophys. Res. Lett.* **31**, No. 11, L11101, 10.1029/2003GL019253, 2004

Lin, J.C., et al., A near-field tool for simulating the upstream influence of atmospheric observations: The Stochastic Time-Inverted Lagrangian Transport (STILT) model, *J. Geophys.Res.* **108** (D16), 4493, 2003.

Pfister, L., et al., Aircraft observations of thin cirrus clouds near the tropical tropopause. *J. Geophys. Res.* **106,** 9765–86, 2001.

Pickering, K., Y. Wang, W.-K. Tao, C. Price, and J.-F. Mueller, Vertical Distributions of Lightning NOx for Use in Regional and Global Chemical Transport Models, *J. Geophys. Res*. **103**, 31,203–16, 1998.

Pittman, J. V., *et al*., Identifying transport pathways into the subtropical lowermost stratosphere during the summertime, *J. Geophys. Res.*, in preparation, 2004.

Poulida, O., R. R. Dickerson, and A. Heymsfield, Stratosphere-troposphere exchange in a midlatitude mesoscale convective complex, 1. Observations, *J. Geophys. Res.* 101, 6823–36, 1996.

Wang P. K., Moisture plumes above thunderstorm anvils and their contributions to cross-tropopause transport of water vapor in midlatitudes, *J. Geophys. Res*. **108**(D6), 4194, doi:10.1029/2002JD002581, 2003.